UNIVERSIDADE D
COIMBRA

DAVID ALEJANDRO DIAZ YANEZ

ENHANCED NANOSTRUCTURED CHROMIUM BASED THICK COATINGS BY HIPIMS

VOLUME 1

Dissertação no âmbito do Mestrado Conjunto Europeu em Tribologia de Superfícies e Interfaces orientada pelos Professor Doutor Ricardo Gil Heriques Serra e Professor Doutor João Carlos Barbas de Oliveira e apresentada ao Departamento de Engenharia Mecânica da Faculdade de Ciências e Tecnologia da Universidade de Coimbra.

Julho de 2022

1 2 9 0 FACULDADE DE CIÊNCIAS E TECNOLOGIA UNIVERSIDADE D COIMBRA

Enhanced nanostructured Cr based thick coatings by HIPIMS

Submitted in Partial Fulfilment of the Requirements for the Degree of European Joint European Master in Tribology of Surfaces and Interfaces.

Optimização de revestimentos espessos à base de Cr nanoestruturados depositados por HIPIMS.

Author

David Alejandro Diaz Yanez

Advisor[s]

Doutor Ricardo Gil Heriques Serra

Professor Doutor João Carlos Barbas de Oliveira

Jury

President	**Professor Doutor Bruno Miguel Quelhas de Sacadura Cabral Trindade**
	Professor at the Universidade de Coimbra
Vowel	**Doutor Manuel António Peralta Evaristo**
	Researcher at Universidade de Coimbra
Advisor	**Doutor Ricardo Gil Heriques Serra**
	Researcher at Universidade de Coimbra

1 2 9 0 UNIVERSIDADE D COIMBRA

tribos

Coimbra, July, 2022

ACKNOWLEDGEMENTS

I would like to express my gratitude to all who have contributed to completing the project described in this thesis.

First and foremost, I would like to thank my advisors, Dr. Ricardo Serra, for constantly providing unconditional support, and all the necessary assistance needed for my work ever since the start of this academic year until the end of this project. To Dr. Joao Oliveira for his unvaluable resources and transfer knowledge that made possible this work. To my laboratory partner and every single person that got involved in the whole journey.

Special thanks to the TRIBOS consortium for providing me with this life-changing opportunity and the European Commission's funding. Extending the gratefulness to all TRIBOS mentors Professor Ardian Morina, Professor Mitjan Kalin and Professor Bruno Trindade for, their support.

Finally, I am earnestly thankful to my parents, siblings who had been my constant source of strength and inspiration through their endless encouragement and motivation.

Abstract

Over the past decade, thin film deposition techniques have improved incredibly. Each new step is a remarkable advance for the technology, but specifically for this industry, each improvement seems to be important for better recognition, which consequently allows better control in sputtering systems. One of these strong techniques on the market is high-power pulse magnetron sputtering (HiPIMS). This can produce coatings with a much denser morphology, a better hardness/elastic modulus ratio, and a smoother surface than conventional thin film deposition techniques.

On the other hand, chromium is one of the most widely used materials in various industries. The importance of Cr for thin film deposition by physical vapor deposition is generally very high due to its excellent performance in surface protection, decorative properties, and very acceptable mechanical properties. It also provides clean deposition processes for the environment, which comes with public safety and health concerns. However, these films are subject to increasing wear and abrasion under harsh long-term conditions.

The work is mainly focused on the development of the deposition parameters of hard Cr coating using HiPIMS, paying special attention in injected percentage of gases for ionization, charges dynamics and impact of soft Cr interlayer to compare thin film morphology, thickness and tribomechanical properties. All deposition systems were operated in DOMS mode using a Cyprium power supply from ZpulserTM LLC.

The effects of injected Argon interlayer deposition on the morphology, thickness and mechanical properties of the achieved coating were studied in detail. Film characterization was performed using scanning electron microscopy, X-ray diffraction and atomic force microscopy.

The previously deposited Cr coatings demonstrated the high ionization capacity of HiPIMS, which was successful in obtaining thick films. Moreover, film growth by continuous bombardment with Cr+ ions resulted in changes in film properties, forming dense microstructure with only a gradual decrease in mechanical film properties.

Keywords Chromium, HiPIMS, DCMS, thick film, Cr coating.

Resumo

Na última década, a técnica de deposição de filmes finos apresentou melhorias significativas. Cada novo avanço marca a tecnologia, especificamente na indústria de filmes finos, onde cada melhoria é também importante para um maior reconhecimento e consequente melhoria do controlo dos sistemas de pulverização. Uma dessas técnicas é a pulverização catódica com impulsos de alta potência (do inglês high power pulse magnetron sputtering, HiPIMS). Neste modo, o sistema consegue produzir revestimentos densos, com melhor rácio dureza/modulo de Young, e superfícies com menor rugosidade do que técnicas de pulverização convencionais.

Por outro lado, o crómio é um material muito usado em variadas indústrias. A importância do crómio na deposição como filme fino por métodos de pulverização é bastante elevada devido às suas propriedades de proteção de superfície, filmes decorativos, e muito aceitáveis propriedades mecânicas. Também oferece um processo de deposição limpo, promovendo as preocupações com a saúde e segurança publica. Contudo, estes filmes apresentam elevado desgaste quando aplicados em ambientes agressivos.

O trabalho aqui apresentado focou-se maioritariamente no controlo dos parâmetros de deposição para obter filmes crómio duros recorrendo ao HiPIMS, prestando especial atenção à percentagem de gás usado para a ionização do crómio, dinâmica de cargas e impacto duma intercamada na melhoria da morfologia dos filmes, espessura e propriedades tribo mecânicas. Todos os sistemas foram preparados em modo DOMS usando uma fonte de potência cyprium da zpulserTM LLC.

Os efeitos do árgon na deposição da intercamada na morfologia, espessura e propriedades mecânicas dos revestimentos preparados foram estudadas. A caracterização dos revestimentos foi efetuada recorrendo à microscopia de varrimento eletrónico, difração de raio-X e microscopia de força atómica.

Revestimentos de Cr previamente preparados demonstraram que a grande capacidade de ionização do HiPIMS permitiu a obtenção de filmes espessos. Do mesmo modo, o crescimento dos filmes a partir de iões Cr^+ resultou em revestimentos densos com moderado decréscimo das suas propriedades mecânicas.

Palavras-chave: Crómio, HiPIMS, DCMS, filmes espessos, revestimentos de Cr.

Contents

LIST OF FIGURES

LIST OF TABLES

LIST OF SIMBOLS AND ACRONYMS

List of Symbols

Ar – Argon

Ar+ – Argon ion

Cr – Chromium

Cr+ – Chromium ion

I – Current

P – Pressure

Ra – Surface roughness

Si – Silicon

V – Voltage

Acronyms

AC	Alternating current
AFM	Atomic Force Microscopy
BCC	Cubic crystalline based
COF	Coefficient of friction
DC	Direct current
DCMS	Direct Current Magnetron Sputtering
DOMS	Deep Oscillation Magnetron Sputtering
EDS	Energy Dispersive X-ray Spectroscopy
FWHM	Full width at half maximum
HiPIMS	High Power Impulse Magnetron Sputtering
HPPMS	High Power Pulsed Magnetron Sputtering
ICDD	The International Centre for Diffraction Data

LC	Critical load
OM	Optical Microscopy
PVD	Physical Vapor Deposition
SEM	Scanning Electron Microscopy
SZM	Structure Zone Model
XRD	X-ray Diffraction

1. INTRODUCTION

Thin film deposition has introduced an incredible variety of techniques and improvements to the engineering industry. This sophisticated and skilled equipment has grown rapidly over the years and its perfect understanding is needed to achieve better materials for more aggressive and different performance conditions in various fields. Equipment manufacturers have made tremendous progress and efforts to improve application conditions, increase requirements and develop more economical deposition systems for successful control of each deposition parameter.

Nevertheless, the overall management of such methods, especially of the deposition variables, is poorly understood. The controversy over which technique provides better results for a particular application is one of the most important issues. A better fundamental understanding of the physics and chemistry of the layers that form will lead to better microstructure applications and new designs of devices in which these coated materials can be incorporated.

HiPIMS technique is associated with the physical vapor deposition (PVD) processes, which involves the ionization of atoms and interaction with the starting material, causing the atoms to be sputtered onto the substrate surface, where they condense into a layer. The mechanism allows the deposition of films even at low temperatures, a better control over the parameters can ameliorate the structure, therefore, properties of the films can be further optimized.

High-Power Impulse Magnetron Sputtering (HiPIMS) is one of the new deposition techniques developed in the last decades, well known to produce a high degree of ionization of the starting material, resulting in much denser films with excellent properties. Further information about the mechanism of this technique is discussed in Chapter 2. However, the deposition rate for this technique is significantly lower compared to other sputtering techniques, which is one of the major drawbacks. HiPIMS produces a superior quality with many other advantages, although, part of the motivation of this research is to gain a deeper understanding of the deposition parameters, film properties and the relation with its growth.

Chrome promises a vast utility on the industry for its further investigation, its high ionization rate for sputtering deposition makes it even more attractive for this particular application, lower shadow effect, less drawback deposition results, and decorative proposes are intensively consider.

Basically, on this project is to explore the enhance of adhesion incorporating an Cr interlayer by Direct Current Magnetron Sputtering (DCMS) and Deep Oscillation Magnetron Sputtering (DOMS) of few nanometres and compare the performance of the 1 μm coatings deposited by DOMS of pure Cr, understanding better the effects on the properties of the films under different deposition modes. The deposited films will be characterized by X-ray diffraction (XRD), scanning electron microscopy (SEM), scratch test, nano-hardness, atomic force microscopy (AFM), profilometry, and pin-on-disk wear test, to correlate the microstructure, morphology, mechanical and tribological properties of the film with the achieved film thickness.

1.1. Objetives

This master thesis project intents to develop a thicker Chromium film deposited on a steel substrate with or without interlayer sputtered by DOMS and DCMS mode, expecting to maintain high density and acceptable tribo-mechanical properties. The principal objectives are listed as follows:

I. Enation of adhesion for a thick Cr coating, implementing two types of sputtering modes for the nano-metric interlayer; DOMS and DCMS to achieve a thicker dense coating using previous referenced studies with same sputtering conditions and deposition technique.
II. Characterization and observation of the substrate bias into the deposited films properties.
III. Quality verification of morphology, thickness and tribo-mechanical properties of the achieved films, throughout discrete tests.

1.2. Thesis Structure

This master thesis has been named as “Hard Chrome Development” which is accomplished as a master research project that takes part of the completion requirement on the Joint European Masters in Tribology of Surfaces and Interfaces. This project focus in considerably thin hard Cr film deposition on a substrate using HiPIMS technique on DCMS and DOMS mode.

The objectives and structure of the master thesis are defined in the first chapter. Chapter 2 contains the background and related literatures under State of the Art, discussing topics as the Cr deposition process on PVD techniques, sputtering effects and challenges in depositing thick Cr films using HiPIMS, the influence of substrate bias, discharged correlation with the film growth, among others. Chapter 3 focus on further details of the carried experimental procedure, while the characterization techniques are thoroughly discussed in the Chapter 4. Chapter 5 is main focused in the results of the whole research. Conclusion and recommendations for future related studies can be found in the Chapter 6.

2. CHAPTER 2 – STATE OF THE ART

As previously mentioned, this chapter contains relevant background information according to the studied matter, being Cr deposition process on PVD techniques, influence of gas concentration in the sputtering environment, discharged correlation with the film growth, and more in-depth overview on sputtering effects and challenges in depositing thick Cr films using HiPIMS.

2.1. Evaporative technologies

Since the main objective here is thin-film formation by deposition, the construction of layers of a few nanometres to about ten micrometres, can be done by a variety of techniques, however, the task of classifying the technologies is made simpler by limiting the number of technologies to be considered. The following is a brief description of evaporation technique.

Probably one of the simplest and oldest technologies lays into the vapor deposition facilities for material coating, this thermal vacuum evaporation is immensely implemented for researchers on the laboratories and dominantly on industry of metal and alloys. The procedure takes place in three basic steps:

1. Generation of vapor due to boiled or sublimed of a source material.
2. Transportation of the vapor particles from the source to the substrate.
3. Condensation of the particles into a solid film on the deposited surface.

Nevertheless, this whole process seems to be extremely simple in principle, but during the performance diverse deposition components must be considered to achieve the best coating conditions for the particular application.

“This variety leads to a large diversity of source components including resistance-heated filaments, electron beams; crucibles heated by conduction, radiation, or rf-induction; arcs, exploding wires, and lasers. Additional complications include source-container interactions, requirements for high vacuum, precise substrate motion (to ensure uniformity) and the need for process monitoring and control”. [1]

2.1.1. Physical Vapor Deposition (PVD)

Physical Vapor Deposition processes are deposition performances at molecular or atomistic scale, which material is transported from the target source in the form of vapor along a vacuum camera or low pressure gaseous (or plasma) environment to the substrate where the particles condense creating a thin film or layer composition on the specimen surface. Generally, PVD techniques are widely used for thin film deposition, layers from few nanometres up to thousand nanometres thickness can be achieve, the facility provides the possibility of multilayer coatings deposition. The deposited morphology of the film varies from flat surfaces to randomly complex geometries, deposition commonly rates between 10 to 100 angstroms (1 to 10 nanometres) per second.

PVD facilities are used to deposit films of elements and alloys as well as compounds using reactive deposition processes. For reactive processes, exist three main obtention procedures, compounds which are formed by the chemical reaction of the deposited material with the environmental gas, compounds formed by chemical reaction with a co-deposited material or can be denominated quasi-reactive formed.

"Quasi-reactive deposition is the deposition of films of a compound material from a compound source where loss of the more volatile species or less reactive species during the transport and condensation process, is compensated for by having a partial pressure of reactive gas in the deposition environment". [2]

2.1.2. Sputtering Deposition

For this form of physical deposition, the vaporized particles from the target are ejected by physical sputtering process. This procedure is a non-thermal vaporization process, means that the ejection of the atoms occurs due to physically momentum transfer from an ionized (energetic particle) bombarding atom that commonly corresponds to a gaseous ion accelerated from plasma.

Considering vacuum deposition, the distance between the target and the substrate in Sputtering is smaller, this technique can be performed by energetic solid bombardment of a solid substrate implementing a vacuum gun or low-pressure plasma, where some particles might experience gas phase impact in the space in between the target and the specimen. The

facility can also be done in high pressure plasma, here the energetic sputtered particles are thermalized by gas phase collisions before its condensation on the substrate surface.[3]

The existence of the plasma in the chamber leads to reactive gas activation, making the inside environment more chemical responsive, this facility is widely applied to thin film metallization, coatings, dry film lubricants, among others.[4]

2.2. Film Materials Sources

One of the great advantages and flexibility of this type of procedures is the wide range of material choices for thin film deposition. The element source is known as target, which material is ejected due to the ionized inert gas atoms onto the surface substrate. To deal with this ejection, the target needs to be exposed to an immense range of energy, that can easily reach up to tens of electron volts (eV).

For the total control of the deposition process, target materials are essential, its ionization rate along with the parameters for the chamber environment, creates a real difference on the obtained coating. Targets are commercially outsourced, that can be found in desirable shapes and elemental composition, since it is made of pure metals, compounds, or alloys.

Alloy targets can be further categorized either as magnetic, non-magnetic, noble metallic, or suitable for high temperature services. Target materials can also be made of compounds or mixture of elements such as oxides, carbides, nitrides, phosphides, or sulphides. It can also be sourced out from pure metals such as Aluminium, Cobalt, Copper, Iron, Magnesium, Manganese, Tin, and Chromium. [5]

2.2.1. Chromium Films

Chromium targets as a pure material have the same properties of the element and therefore the same possible applications in the industry, mainly used for corrosion resistance, average wear resistance comparing to other metals, decorative purposes such as shiny finishes, high hardness, low coefficient of friction and an overall tribo-mechanical acceptable properties in mechanical performances.

Due to some environmental and health restrictions Chrome coatings have been studied for specific application such as thermal spraying [6], or coatings with mixed elements to reduce the undesirable effects on health [7] although, some industrial applications are still developed for different typical or actual performances, some examples are corrosive or oxidation resistance [8], solar energy [9], and better mechanical performances.

Those listed examples above correspond to resulted procedures under specific deposition parameters, thus understanding the achieved properties, behaviour, and microstructure films. One well known deposition procedure that has an historical data is hard chrome plating, due to reduce production costs, high levels of effectiveness, and remarkable anti-corrosive and wear properties, nevertheless, it presents some inconveniences as well, as instance low electrolytic rate, toxicity and lower deposition rate comparing to other techniques.[10]

For all that, the implementation of Chromium for electrochemical techniques has been restricted in the industry, to mainly avoid whatever kind of problematics with health and safety concerns; Regarding this topic further information is presented on the coming chapters.

2.3. Deposition of Chrome films by HiPIMS

In the following part, the principal explained technique is High Power Impulse Magnetron Sputtering focusing on the drawbacks background using this facility, the benefits to implement this deposition system for thin films, the importance and possible impact of the manipulation of noble gases for the performance and the feasible relation between discharge deposition dynamics into the film growth.[11]

2.3.1. Magnetron Sputtering

This form of deposition accomplishes the sputtering by decreasing the discharge voltage and expand the operational pressure rate, in other words it applies magnetic fields, therefore, the lifetime of the electrons near the target increases, capturing the ionized

electrons on the substrate vicinity and raise the intensity on the cathode. The basics of the procedure in planar discharge is shown in the next figure 1.

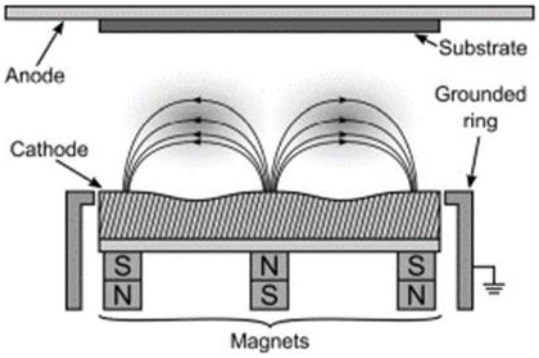

Fig. 1. Planar magnetron discharge scheme for sputtering.[12]

In planar magnetron the cathode can present a circular plate shape or rectangular plate, this form of configuration can create a balanced magnetic field by non-variable magnets with the particularity that the middle magnet has a diverse polarity comparing to its neighbours, producing an inside opposite polarity. The magnetic field lines go out from the centre of the cathode and go back into the cathode at the annular.

The electrons would spend more time in the perpendicular region to the magnetic field, being the ideal geometry to have the magnetic field parallel to the cathode surface. However, as can be seen from the previous figure, the field lines are compromised by magnetic field of the magnets, extending them from the sputter surface and return, creating an arc which is referred as the ionization region. Within this arch, ionizing electrons and ionized gas are confined forming a dense glow discharge and consequently a high level of sputter activity

This enhancement of the ionization rate or sputtering yield inside the chamber, occurs principally due to the implementation of the magnetic field, that leads to higher deposition rates and gives the huge advantage to operate with low working gas pressure, lower than four Pascals according to previous research. [13]

2.3.2. High Power Impulse Magnetron Sputtering (HiPIMS)

Considered one of the most recent techniques in the industry of films deposition, it uses unipolar mode, referred to as high power impulse magnetron sputtering, due to its superiority highly ionized flux on the sputtering material meanwhile maintains low limits

damage due to power target magnetron, this performance has been proposed as the future of thin film deposition.

In HiPIMS, this is accomplished using pulsed plasma discharges with a peak power density in the range 0.5 – 10 kW/cm2 (averaged over the target surface) at a low duty cycle in the range of 0.5 – 5%, that is, considerably lower than the 50 – 90% in pulse magnetron sputtering. The HiPIMS discharge operates by applying square voltage pulses of about 500 – 2000 V, which generates peak current densities of up to 3 – 5 A/cm2 [14] The pulse length is in the range 20 – 500 μs, but typically 30 – 100 μs when depositing thin films, with a repetition frequency of 50 – 5000 Hz. [12]

Since it implements highly power densities in the magnetron cathode target, presents a visible increase in the charge carrier density during the pulse, this means that the electron density in the ionization region is very close to the target surface on the order of 1018 – 1019 m−3 which corresponds to ionization impact for a sputtered metal atom on the order of 1 cm or less. [15]

With such order of electron density in the discharge, a significant fraction of the sputtered material has the possibility to be ionized making it a fundamental feature of HiPIMS. [16], [17]

2.3.3. Collision Gases

Basically, glow discharge holds some particles in, like electrons, different types of ions, neutral atoms, and molecules, as well as photons. The collision or interaction between all of the previously mentioned species must be contemplate in principle, however, some interactions are more predominant and crucial than others, especially for low pressure types of glows for sputtering applications.

One of the most important parameters in the discharge physics is the working gas pressure, since at low pressure, only a few collisions may occur, and the total energy transfer between species is inefficient. On the other hand, at high pressure, many collisions can occur between the various plasma species, which result in more equal temperatures of the particles in general.

For argon gas at 0.13 Pa (1 mTorr) and room temperature, the average distance travelled by an Ar atom before a collision to another Ar atom is about 8 cm, and most other gases are within a factor of three of this value (provided gas atoms of thermal energy). [18]

When two particles collide, one or both particles may change their momentum or their energy, neutral particles can become ionized, and ionized particles can become neutral. Collision processes can be divided into elastic and inelastic collisions, depending on whether the internal energies of the colliding particles are maintained or not. The total energy, which is the sum of the kinetic and potential (internal) energy, is conserved in a collision. When the internal energies of the colliding particles do not change, then the sum of kinetic energies is conserved, and the collision is said to be elastic. When the sum of kinetic energies is not conserved, the collision is referred to as inelastic.[19]

The inelastic collisions often involve excitation or ionization of the colliding particles, so that the sum of kinetic energies after collision is less than that before collision. Inelastic collisions involving electrons are essential to the maintenance of a glow discharge. The most important of these collisions is electron impact ionization. For electron impact ionization of an argon atom, this is written:

$$e + Ar \longrightarrow Ar^{+} + 2e,$$

Eq. 1. Impact Argon ionization.

After the particles interaction. Argon is obtained with two electrons, therefore, an electron bound is ejected from the atom. Thanks to this multiplication of free electrons and its acceleration by the electric field, the glow charge remains itself. It is referred to as excitation when a transfer of energy to a bound electron on the atom allows the electron to jump to a higher energy level within the atom with a corresponding quantized absorption of energy. For ions colliding with atoms, the main processes are elastic scattering in which momentum and energy are exchanged.

The most important inelastic collisions are listed in Table 1. [12]

In molecular gases, there are a number of additional important processes that can occur. These may include inelastic collisions, such as vibrational and rotational excitation, dissociation, and dissociative recombination. When negative ions are present, the processes can include attachment, detachment, ion–ion mutual neutralization, and positive–negative ion charge transfer.[20]

Tab. 1. Most important inelastic collision types in glow discharges. Chemical symbols are used where appropriate. M refers to any type of metal atom and e refers to an electron.

Inelastic reaction	Reaction example	Comments
Ionization	$e + Ar \longrightarrow Ar^+ + 2e$	A bound electron in the atom is ejected from the atom. Threshold energy for ionization to occur (ionization potential ϕ_{iz}). For Ar, $\phi_{iz} = 15.76$ eV.
Excitation	$e + Ar \longrightarrow Ar^* + e$	Excitation of a bound electron to a higher energy level within an atom. Threshold energy for excitation to occur. For Ar, $\phi_{exc} = 11.56$ eV.
Recombination	$e + Ar^+ + body \longrightarrow Ar + body$	Inverse of ionization. Three body collision (with a wall for example) is typically required.
Relaxation	$Ar^* \longrightarrow Ar + h\nu$	Inverse of excitation. Release of photon with energy $h\nu$.
Dissociation	$e + O_2 \longrightarrow O + O + e$	Breaking apart a molecule. Requires overcoming the bond strength in the molecule, which is 5.15 eV for oxygen.
Dissociative electron attachment	$e + O_2 \longrightarrow O^- + O + e$	Often the primary mechanism for negative ion formation in molecular gas. For oxygen, the threshold energy for dissociative attachment is 4.2 eV.
Charge transfer	$Ar + Ar^+ \longrightarrow Ar^+ + Ar$	Ion-neutral collision.
Penning ionization	$Ar^m + M \longrightarrow Ar + M^+ + e$	Involves long-lived excited species called metastables, such as Ar^m with energy levels at 11.56 eV and 11.72 eV.

2.3.4. DC glow sputter source

The upper electrode is the cathode, which serves as a target for ion impact sputtering. In sputter deposition the cathode surface (the target) is the source of the film forming material. The material is then transported through the low-pressure gaseous environment before it condenses on a substrate to form a film. Such processes can be used to deposit thin films of elemental, alloy, and compound materials as well as some polymeric materials. On the next Fig. 2. It is shown a scheme of this setup.

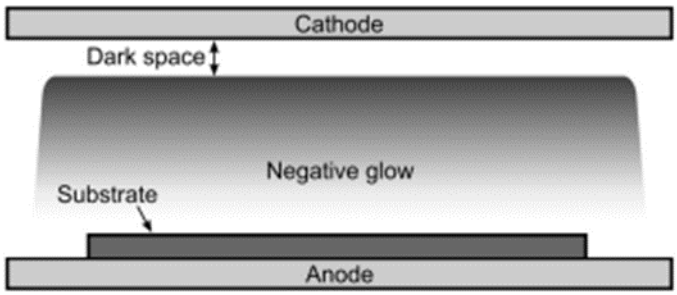

Fig. 2. Sputtering glow discharge with low aspect ratio.

For sputter applications with the dc glow discharge, the distance between cathodes and anode is generally short, so that normally only a short anode zone is present along with the cathode dark space and the negative glow, where the slightly positive plasma potential returns back to zero at the anode. Cathode diameters are typically in the range 10 – 30 cm, whereas the spacing between the cathode and anode is 5 to 10 cm. This configuration is referred to as an obstructed dc glow discharge. [12]

A typical dc glow discharge is maintained by secondary electron emission, and the operating pressure must be high enough so that the secondary electrons are not lost to the anode or to the grounded surfaces before performing ionization. These pressures are higher than preferred for optimum transport of the sputtered atoms due to scattering by the working gas atoms.

The disadvantages of dc diode sputter deposition include low sputter rate and thus low deposition rate, target poisoning by reactive contaminants, substrate heating due to electrons accelerated away from the cathode target, and that only electrically conductive

materials can be used as sputter targets. Also, the sputter power efficiency (sputtered atoms/ion-volt) is relatively low in these discharges as they operate at high voltage, and this efficiency decreases with increasing energy.

2.3.5. Sputtering effects

Some disadvantages can be achieved using sputtering techniques, since the bombardment with ionized particles can transmit several effects in the surface region of the substrate. As can be seen in the Fig.3. few undesirable interactions between particles may occur in different regions of the surfaces depending on the collision energy and transferred momentum of each specie. This highly energy interaction in HiPIMS, can possibly affect the deposition rate on the procedure, by two consequences, either high energy sputtered atoms or high energy reflected neutrals of the bombarding gas.

In several circumstances, unpleasant re-sputtering can be achieved on the deposited material by high energy of particles impinging on the growing film that consequently exceeds the sputtering threshold of the target material. On the other hand, the highly energetic bombardment of neutral films may cause disagreeable defects on the surfaces, such as dislocation which are a consequence of residual stresses on the film growth. Another possibly effect is the preferential deposition in the film growth, this result is considered as substrate related and can be obtained by preferential growth of atoms forming hills on the surface, this reaction is also known as shadowing effect. [21]

Unfortunately, this outcome contributes to under dense regions, typically valleys or surfaces that are not perpendicular with the incident deposition flux, resulting to formation of columnar microstructure. Deposition at higher bombardment energy however reduces the formation of atomic shadowing.

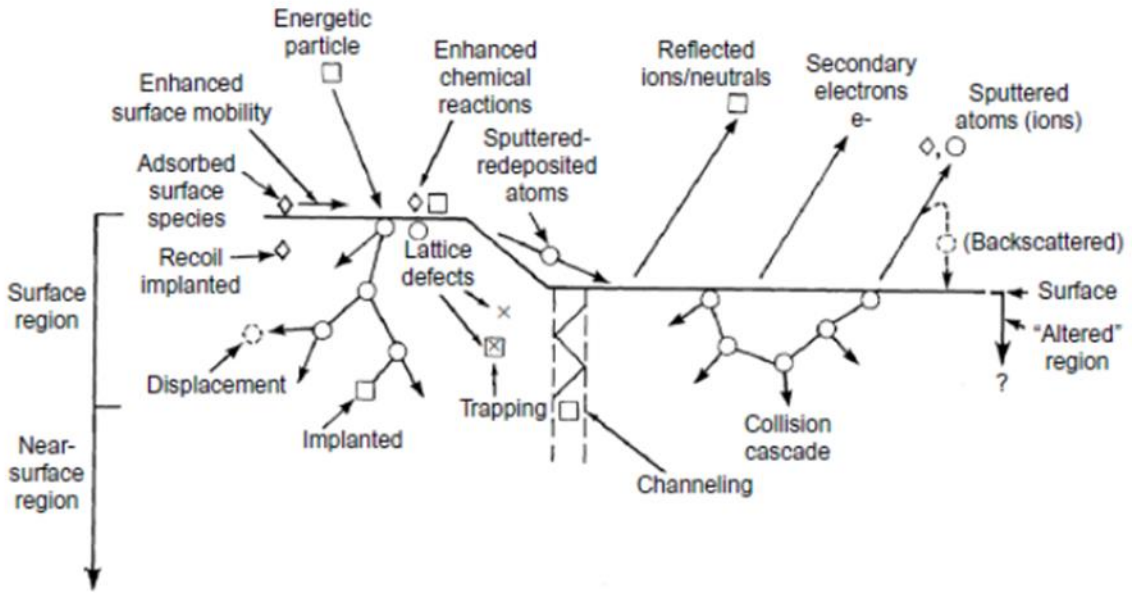

Fig. 3. Bombardment particle interaction by energized atoms in the surface region.[22]

In addition to this problematic from the sputtered particles, some consequences can also appear from the target material as well. Under specific circumstances, the bombardment can be done in the opposite direction, causing a self-sputtering in the target. Obviously, the deposition rate or deposited particles on the surface decreases significantly due to this inconvenient. High target voltages deposition additionally, presents higher ionization rate of sputtered atoms and increased probability of ions returning back to the target due to the increased ion retarding potential in the target area. Both effects prevail at high peak power as they are influenced by the peak current and peak voltage, typically used in HiPIMS. [23]

Deposition applied parameters likewise contributes significantly to the freely film increase, being tremendously important the outcome regarding the morphology and the microstructure in the final sputtered film. The fundamentals of the film growth and the microstructure according to the applied temperature is basically understood by the structure zone model (SZM) published by Thornton. [24]. Fig. 4. Shows the microstructure growth model.

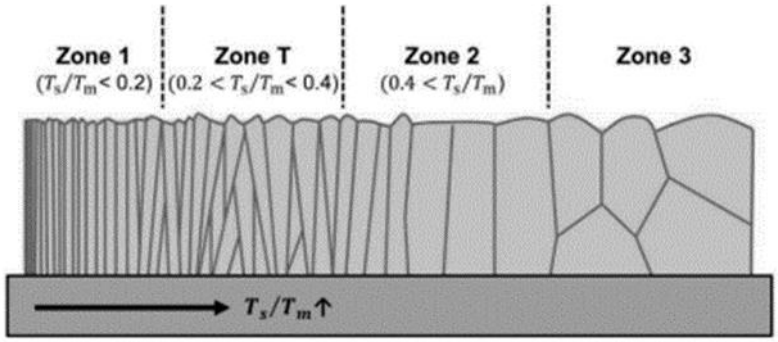

Fig. 4. Structure zone model of a thin film grown a function of temperature ratio.

Reducing the substrate's temperature during growth will be effective to minimize the surface diffusion of the adatoms. According to the structure zone model the morphology of a thin film is classified depending on the ratio between the substrate's temperature TS and the melting temperature of target material Tm during growth.[25],[26], [27]

Finally, the above listened effects are the most common in HiPIMS sputtering, although, more can be expected and highly achievable specially in high voltage conditions.

2.4. Substrate Bias

The proposed method to sputter the substrate is an ionized physical vapor deposition process, the sputtered material is expected to be highly ionized, this means that applying in the substrate bias voltage the collected energy of these ions can strike the substrate in a controlled way.

The substrate bias voltage can thus be a key parameter during film deposition since bombarding energetic ions enhance adatom migration, promote desorption of physically adsorbed atoms and shallow ion implantation, and trap impinging atoms. [28]

Thus, there are two important issues that need to be kept in mind while discussing substrate bias in HiPIMS:

• The largely neglected issue of a drop in the applied substrate bias voltage during the HiPIMS discharge pulse, which prevents the user from maintaining a desired bias voltage. It also leads to the obvious question of what bias voltage was actually used during deposition.

• The possibility to synchronize a pulsed substrate bias with the HiPIMS discharge pulse to selectively attract certain ionic species, that is, bias optimization in the time domain.

2.4.1. Bias Solutions

During the discharge pulse, the plasma density increases (approximately in proportion to the discharge current), which loads the bias power supply down as any deviation from the floating potential requires more and more current drive. In HiPIMS, this load arises from the considerable ion flux generated. Under these conditions, the bias voltage drops due to the gradual discharge of the smoothing capacitance internal to the bias power supply and also due to the voltage drop over the output impedance of the power supply. The inductive drop can be seen in the recovery of the bias voltage as the bias current rapidly decreases after the pulse. In some types of power supplies made for driving plasma discharges, the rapidly changing current can also trigger arc suppression features in the power supply.[24][28], [29]

After the pulse, the plasma density decays rapidly, and the substrate load quickly becomes a very high impedance. Now the average bias voltage increases as the slowly changing supply current recharges the smoothing capacitance. As the voltage control loop in the bias power supply loses control of the output voltage, there may be an overshoot or ringing in the bias voltage as control is regained, depending on the damping behaviour of the loop. The large majority of power supplies used for substrate bias are only one-quadrant supplies, meaning that they can only draw current from the substrate and that any overvoltage will only slowly be bled away from the output by leakage resistances.

A simple remedy to reduce the time constant of the high-impedance load is to add an external shunt resistance of suitable size. The behaviour of the bias voltage changes somehow in character when using midfrequency pulsed dc voltage for substrate bias, but the problem of reduced bias voltage when the ion current is large during the pulse remains. Pulsed dc power supplies tend to be good low-impedance voltage sources as required to drive high-frequency pulses on a capacitive plasma load, but they also tend to have more sophisticated arc-suppression features compared to most dc power supplies, and this increases the risk of false detection of arcs due to the high ion flux density during the HiPIMS pulse.

With higher pulsed bias frequencies, such as when using a rf source, there is still the issue of the bias voltage dropping during the HiPIMS discharge pulse. This is due to self-biasing (negative charging) of the substrate table due to the impinging electrons in combination with a blocking capacitor in the rf circuitry, which does not allow the charge collected on the substrate table to discharge to ground. The way the self-bias builds up by rectifying properties of the plasma along with heating of the electrons, rather than the straighter rectification at lower frequencies, means that the bias voltage is much more sensitive to the plasma conditions at the substrate table.

There is also the issue of how much of the rf power provided by the generator is actually absorbed by the plasma due to the matching between generator and plasma. The change in plasma properties between a quiescent, fully rf-driven plasma, and the high-density HiPIMS plasma is so large that both the rf power required to drive the desired self-bias and the matching conditions are vastly different at different times. This makes the rf bias method the most difficult one to use in a HiPIMS process. In fact, when applying rf bias (13.56 MHz), the bias voltage can be observed to drop completely to zero very early in the pulse and stay low for a long while afterwards. One challenging way to some-what remedy this issue is synchronizing the rf bias with the HiPIMS pulse.[30]

The key to successfully generate a well-defined bias signal or bias pulses during HiPIMS operation is to present the substrate with a low-impedance voltage source, switched on and off by a fast switch. A low-impedance voltage source is most easily achieved with a regular dc power supply and a smoothing capacitance that can handle the pulse current without too much drop in the output voltage. The smoothing capacitance necessitates some form of arc-limiting function to prevent the energy stored in the smoothing capacitance from being dissipated through a substrate arc. A convenient way of handling arcs is to use the bias switch to disconnect the bias source in case of an arc. [12]

2.4.2. Synchronized pulsed HiPIMS bias

It is well known that rare gas ion bombardment of the growing film during conventional sputter deposition is widely employed to increase film density [24], improve film/substrate adhesion via interfacial mixing [23], enhance crystallinity [29] and so on. However, at high ion energies, such ion bombardment leads to detrimental residual ion-induced compressive stress of several GPa [21], [31] On the other hand, in HiPIMS, it is

straightforward to generate a substantial metal ion flux to the substrate in addition to the working gas ions. Furthermore, studies of mass, flux, and energy distribution of each ion species incident at the film growth surface have shown that there is a significant difference in arrival time of the ionic inert working gas versus metal species. [32][33], [34]

One solution is synchronizing the substrate bias to only the metal ion-rich portion during the HiPIMS pulse. This requires the user to select when to activate a bias pulse with respect to the HiPIMS discharge pulse (i.e., a delay of the bias pulse in the time domain) and repeat the process at a common frequency. Such operation is schematically shown in Fig. 5, where a proper HiPIMS substrate bias, with a constant pulsed bias voltage, is synchronized to the HiPIMS discharge voltage pulses on two magnetron targets. Note that there is a (user-defined) delay between the onset of the HiPIMS voltage pulse and the HiPIMS substrate bias voltage pulse, as seen in Fig. 5B. Furthermore, one can also combine such synchronization of the substrate bias voltage with co-sputtering compounds from several magnetrons. In such a configuration, it is desirable to individually synchronize the magnetron sources and the substrate bias source as in Fig. 5.

A more sophisticated solution is to not only synchronize the bias timing with the sputter sources, but also to apply different voltages at different times. If only square voltage pulses of different amplitudes are needed, then we can simply repeat the bias pulsing described earlier with different pulsers set to different voltages. If full wave form control is needed, then a high-bandwidth voltage source must be used instead, which can be cost-prohibitive. [12]

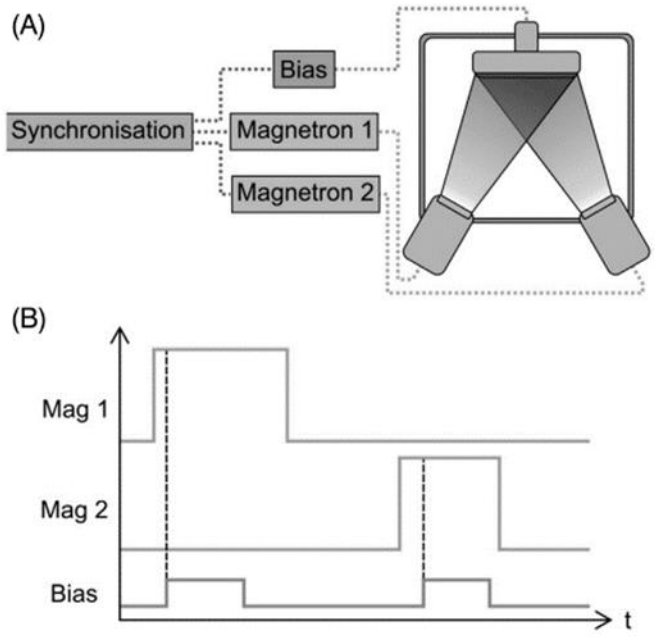

Fig. 5. Synchronized HiPIMS operation. (A) A schematic illustration of how to set up synchronized HiPIMS on two magnetron targets for co-sputtering, including synchronization of the pulsed HiPIMS bias voltage. (B) An example of the synchronized output voltage signals in time for the setup given in (A).

2.5. Industry and Environment concerns

Metals occur naturally in the environment in varying concentrations and are present in rocks, soil, plants, and animals. All metals at high concentration levels have negative impacts because they are easily accumulated. Cadmium, mercury, lead, copper, and zinc have received special attention in ecotoxicology in recent years. Some metals are necessary for the biological functions of organisms (e.g., cobalt, copper, manganese, molybdenum, zinc, and chromium). They occur in different forms: as ions in water, as vapours, salts or mineral rock, sand, and soil. They can be bound by organic or inorganic molecules or attached to particles in the air. Both natural and anthropogenic sources emit metals into air and water.[35],[36]

Excessive levels of metals in the marine environment can affect marine biota and are hazardous to human consumers of seafood. During the recent three decades considerable attention has been given to problems concerning negative effects of heavy metals on various

ecosystems in different environmental compartments. Numerous field observations indicate a significant increase of heavy metals concentrations in agricultural and forest soils as well as in marine and inland water sediments. An assessment of the potential ecological and health risks associated with atmospheric fluxes of heavy metals requires an understanding of the relationship between sources of emission to the atmosphere and the levels of the concentrations measured in ambient air and precipitate.[37]

Chromium is one of the heavy metals whose concentration in the environment is still increasing. It does not need to be worried about global risk of chromium contamination, but for local environments it could be a serious problem. Since the Chrome utilization in the industry has been carried for a long term in history, vary publishments have been carried on demonstrating the influence of this element on the human health and the impact that can generate in the industry due to its utilization. Most of the articles talk about the toxicity of this element in the human cells, being hexavalent chromium highly risky to carcinogens concerns. However, further investigation was done in other fields such us, biomonitoring, chromium sources, exposure, analytical chemistry among others. [38],[39],[40]

2.5.1. Uses of Chromium

Chromium is resistant to ordinary corrosive agents at room temperature, which explains its uses as an electroplated, protective coating. It is also used in ferrous and nonferrous alloys, in refractories, and in chemicals. Ferrous alloys, mainly stainless steels, account for most of the consumption. These steels have a wide range of mechanical properties as well as being corrosion and oxidation resistant. Cast irons may contain from 0.5% to 30% of Cr, which provides hardness, toughness, anticorrosive properties, and wear resistance.[41]

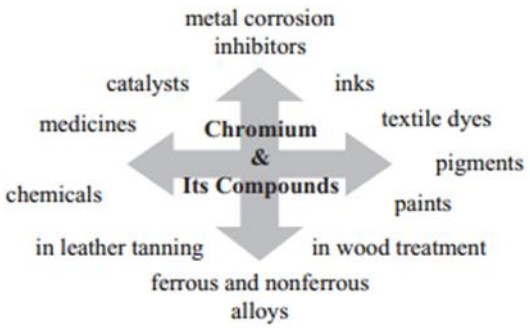

Fig. 6. Uses of chromium and its compounds.

Chromium is also widely used in nonferrous alloys (nickel, iron-nickel, cobalt, aluminium, titanium, and copper). Chromium chemicals are used in a variety of applications. The largest amount is consumed to manufacture pigments for use in paints and inks. Other applications include leather tanning, metal corrosion inhibition, drilling muds, textile dyes, catalysts, wood, and water treatment. Chromite is used in the refractory industry to make bricks, mortar, and ramming and gunning mixes. Chromite enhances their thermal shock and slag resistance, volume stability, and strength. [42]

2.5.2. Toxicity of hexavalent Chromium

Severe and often deadly pathological changes are associated with excessive intake of Cr (VI) compounds. It has been found that occupational exposure to hexavalent chromium compounds leads to a variety of clinical problems. Inhalation and retention of materials containing Cr (VI) can cause perforation of the nasal septum, asthma, bronchitis, pneumonitis, inflammation of the larynx and liver and increased incidence of bronchogenic carcinoma. Skin contact of Cr (VI) compounds can induce skin allergies, dermatitis, dermal necrosis, and dermal corrosion.[43]

Chromium (VI) connected with long-term occupational exposure (such as workers in the chromate industry) is a chemical carcinogen that can cause carcinomas of the bronchial systems. Epidemiological studies of workers working at the chromate industry have found a large increase in bronchogenic carcinomas among workers involved in the isolation and manufacture of dichromats from ores. The mechanism of cancer formation caused by Cr (VI) is not known for certain; however, it has been postulated that Cr (VI) binds to double-stranded deoxyribonucleic acid (DNA), therefore altering gene replication, repair, and duplication.[44]

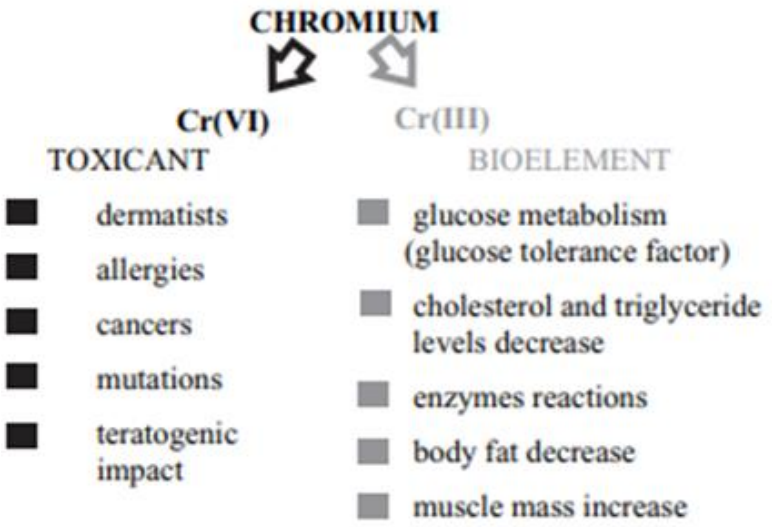

Fig. 7. Chromium valence effects on humans.

However, these problems are not restricted to chromium-industry workers. During the process of production, a relatively large quantity of chromium is released to the atmosphere, earth, lakes, and rivers. Hexavalent chromium in air is a human carcinogen and toxicant. In soil and water, the less toxic Cr (III) ion can be oxidized to carcinogenic, teratogenic, and mutagenic Cr (VI). It is generally assumed that in living organisms only the reduction process Cr (VI) to Cr (III) takes place.[37], [45]

Not only toxicity, but also the mobility and bioavailability of chromium, depend fundamentally on its chemical form. Cr (VI) compounds are usually highly soluble, mobile, and bioavailable compared to sparingly soluble trivalent Cr species.[46]

3. CHAPTER – EXPERIMENTAL PROCEDURE

3.1. Overview

Using previous analysed and studied data from preceding investigations [47], this work focuses on the possible impact of an interlayer enhancement for a better mechanical and tribological performance of the overall pure thick Chromium coating, furthermore, for this particular HiPIMS technique.

3.2. Deposition Procedure

The metallic substrates used in this work were manually polished before the deposition. Just before the start of Cr deposition manually cleaning in the surface was done, using ethanol and acetone for all samples. Surface activation step was achieved inside the vacuum chamber using etching parameters at 0.5 Pa for all the depositions, using pulsed DC power supply with 280 W at 120 kHz and 1616 ns using 350 V of substrate polarization. Increase of etching time was tested in one sample. During the etching step a chromium target was used to generate ions running in DCMS process at 250 W, 330 V and 0.8 A, with a shutter superimposed between cathode and substrate to prevent film deposition.

After the etching process an interlayer was deposited. The different interlayer condition used can be easily defined, two systems were deposited without interlayer but using increasing impinging time before Cr layer, then, other two samples possess increasing thickness of Cr interlayer with estimated density fixed (DCMS) and finally, one more system with Cr interlayer of higher density (DOMS).

For the samples with fixed density interlayer, for 100 nm 2.5 minutes deposition was caried, and for 200 nm, 5 minutes was estimated, both sputtered at 0.5 Pa and 1200 W using DCMS process together with -60 V of substrate bias. The third interlayer system used DOMS at 0.5 Pa and 1200 W. DOMS pulse characteristics were 1052 V, 60 A, 230 Hz and -60 V of substrate bias.

Finally, using a Chromium target, similar 1 micron chromium film is deposited in all the samples for 40 minutes to get the desirable thickness, 20 standard cubic centimetres per

minute (sccm) of Ar gas at 0.5 Pa pressure inside the chamber, and without bias applied on the substrates. A resume of the interlayer conditions is shown in table 2 and the deposition conditions used for Cr film follows in table 3.

Tab. 2. General interlayer deposition plan for the samples.

	Cr inter 01	Cr inter 02	Cr inter 03	Cr inter 04	Cr inter 05
DCMS Etching	10'	30'	10'	10'	10'
Interlayer mode	x	x	DCMS	DCMS	DOMS
Interlayer thickness (nm)	x	x	100	200	100

Tab. 3. Specific deposition parameters for all Cr inter samples.

	Deposition	
Film	Voltage (V)	Current (A)
Cr inter 01	1327	98
Cr inter 02	1301	96
Cr inter 03	1343	98
Cr inter 04	1359	97
Cr inter 05	1314	98

Tab. 4. General thick Cr deposition conditions.

	Cr thick 1	Cr thick 2	Cr thick 3	Cr thick 4
Interlayer thickness (nm)	x	100	100	x
DOMS 400V (1 µm)	40'			
DOMS + substrate bias -60V	80'	80'	160'	160'
Final thickness (µm)	3	3	5	5

Tab. 5. Specific deposition parameters for all Cr thick samples.

	Deposition		Substrate bias	
Film	Voltage (V)	Current (A)	Voltage (V)	Current (A)
Cr thick 1	1341	98	59	5
Cr thick 2	1351	101	58	5
Cr thick 3	1351	100	59	5
Cr thick 4	1338	99	59	5

The selected conditions to produce thick coatings consisted in two samples with the selected interlayer and two other samples without interlayer to be used as reference. In all samples a 10-minute etching step was performed, and in the two systems with interlayer, a 100 nm interlayer was deposited using the same conditions as in Cr inter 05 sample (Table 1).

The Cr film starts with DOMS sputtering for about 40 minutes, which corresponds to one micron approximately, followed by 80 minutes or 160 minutes Cr DOMS with

substrate bias of -60 V, to achieve 3- and 5-micron total thickness chromium films. The work main goal is to achieve thick Cr films maintaining high density throughout its thickness.

4. CHAPTER 4 – CHARACTERIZATION TECHNIQUES

4.1. Mechanical Film Properties

As referred previously adhesion of films is an important feature to ensure that films can handle tribologically testing for a set of first experiments. Thus, the adhesion of the films will be evaluated using the scratch test apparatus – a Rockwell C indenter with spherical tip radius of 0.2 mm and conical angle of 120°. The scratch test was applied on Cr films deposited on AISI M2 steel substrates. The normal load will be linearly increased from 3 to 70 N (scratch speed of 10 mm/min) to generate a controlled scratch. Optical microscope analysis will be used a Leica DM4 B vertical imaging to evaluate the critical load and assess the mode of coating adhesion, according to standard scratch test evaluation. The critical load data will be used to quantify the adhesive properties of the film.

Film hardness and Young's Modulus were obtained by nano-indentation technique (Micro Materials NanoTest) using a Berkovich diamond pyramid indenter. Evaluation of hardness was performed from load-displacement curve using the depth-sensing mode. To keep the indentation depth to less than 10% of the thinnest film, only the recorded values from 5 mN were used for the thin-interlayer coatings, and for the thicker films 20 mN was applied. The indentation loads to be presented in this work were selected to avoid any possible effect from the substrate.

4.2. Surface morphology and chemical composition

The roughness and topography of films were investigated using Bruker Innova atomic force microscopy (AFM) in contact mode. Applied cantilever is made of silicon material with a nominal tip radius of 6 nm at a frequency of 300 KHz. Multiple 2 x 2 μm areas were scanned on each film to ensure proper representation of the sample surface. The

statistical quantities were obtained from the AFM scans using the Gwydion software (version 2.58) after levelling the surface.

The chemical composition of the coatings is evaluated by Energy Dispersive X-Ray Spectroscopy (EDS). Scanning Electron Microscopy (SEM) will be used to examine the fracture cross section and surface morphology of the coatings, using Quanta 400FEG ESEM system with 2 keV beam to acquire micrographs in several surface and cross-sectional areas of Cr films. Surface analysis after pin-on-disk testing was performed in Hitachi model SU3800 coupled with Bruker Quantax Compact EDS detector.

4.3. Film Structure

Analysis of film microstructure was performed through X-ray diffraction (PANanalytical X'Pert PRO MPD) in θ–2θ geometry of parallel beam using Cu Kα radiation (45 kV and 40 mA). The XRD equipment was mounted with parallel plate collimator (0.7°) and Soler slits (0.004°) on the path of the diffracted beam, and a hybrid monochromator (with a Cu W/Si mirror and a double crystal Ge (220)) on the incident beam optics. X-rays were collected using a PIXcel detector in receiving slit mode. The films were scanned from 30° to 140°. The recorded XRD spectra were fitted using a pseudo-Voigt2 function to obtain the corresponding values of peak position (2θ) and full width at half maximum (FWHM). The generated peak intensities from each pattern were then divided by the relative intensities from powder ICDD card of Cr resulting to the measured relative intensities of the intense peaks.

The calculation of the deflection induced by Cr film-substrate, was carried by measure the residual stresses (based on Stoney equation – which relates the curvature of the system and stress) [30], [48] will be performed on a 2D mechanical Profilometer. The residual stress induced on the Cr films was measured based on the resulting total curvature after film deposition. Measurement of curvature radius of all films was obtained using an optical profiler (Mitutuyo Surftest SJ-500) in two orthogonal directions along the x and y axes.

4.4. Tribological film behaviour

The coatings that were selected as appropriate throughout several tasks will be tested at room temperature in an ambient air, dry contact-controlled atmosphere of 21 degrees Celsius and 40% of humidity, the coefficient of friction is continuously acquired. Steel balls AISI 52100 with a diameter of 10 mm were used as counterparts, these balls are standardly used to ensure high hardness with which the wear volume loss of coatings will be overestimated in relation to the expected loss in actual service conditions. All tests were performed with a normal load of 3 N, sliding speed of 0.1 m/s, and duration of 26,550 cycles resulting to a total distance of 1000 m.

Wear rate of the coatings will be determined from the area of the wear track cross section using a surface profilometer (Mitutuyo Surftest SJ-500) to measure the volume loss due to wear (mm3) and calculate the specific wear rate (mm3/Nm) in accordance with Archard's law for calculate the wear rate of the worn steel balls used on the characterization.

Finally, the tested worn surfaces and wear debris will be investigated by SEM and EDS.

5. CHAPTER 5 – RESULTS

This work was divided into two experimental stages, the first one was focused on the investigation and development of a thin nano interlayer having different possible options, and the second stage consisted in the testing of thicker Chromium films with the selected interlayer.

5.1. INTERLAYER DEVELOPMENT

5.1.1. Film Structure

On the following graph 1, all the diffractograms for the Chromium deposited interlayers are compiled, showing obvious dominant peak indexed (110) family of planes of BCC Cr crystalline structure. As was mentioned before, all the samples have 1 micron

chromium film thickness. The (110) peak intensity shows some variation dependent on the interlayer conditions. Substrate silicon peak can be seen as well in the diffractograms corresponding to the (400) family of planes.

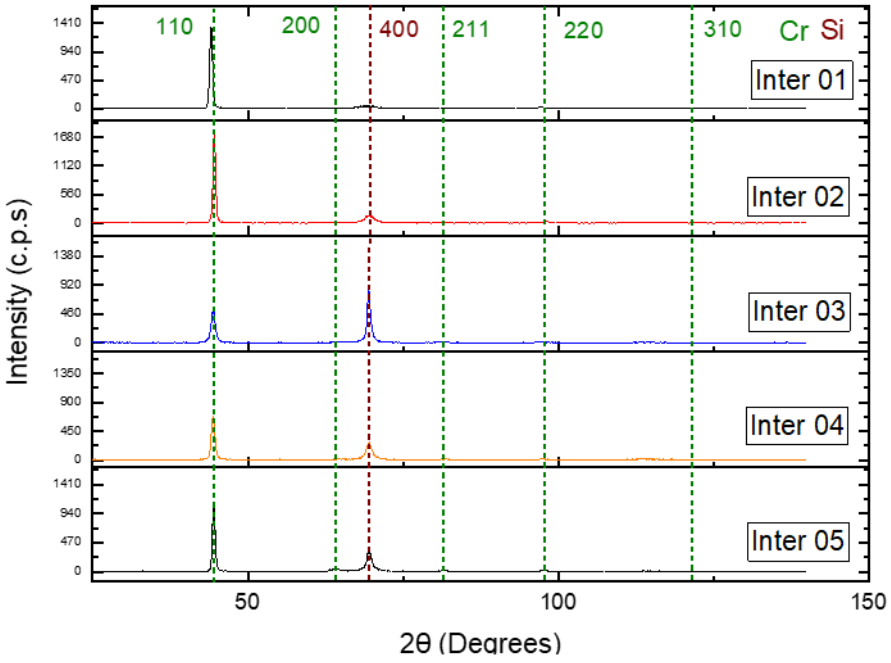

Gph 1. Diffractograms compilation for Cr inter samples.

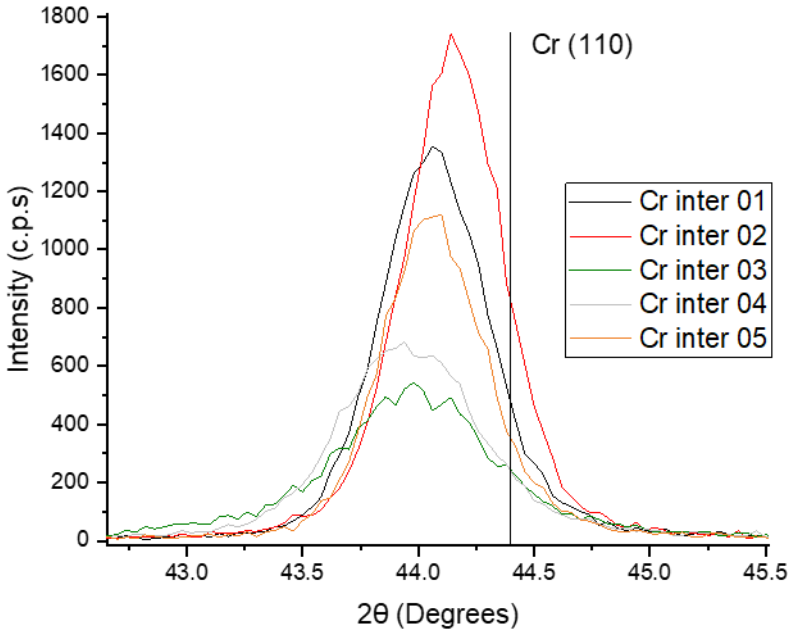

Gph 2. Cr inter Chromium peak (110) diffractogram comparison.#

To better identify the peak shift, higher resolution scan of 110 Cr single peak for every specimen was plotted. The results present in the graph 2, shows a clear peak shift for all samples comparing with the Cr chromium peak pattern position (ICCD 00-006-0694). Samples with DCMS interlayer (Cr inter 03 and 04) loses about one third of intensity comparing to the most intense one among them which is Cr inter 02, besides, those samples present bigger peak shifting to lower degrees in the spectra. The Cr inter 05 has some peak shifting but the intensity is one third lower comparing to the highest one. The graph 2 indicates that the DCMS samples are the most shifted peaks in the spectra.

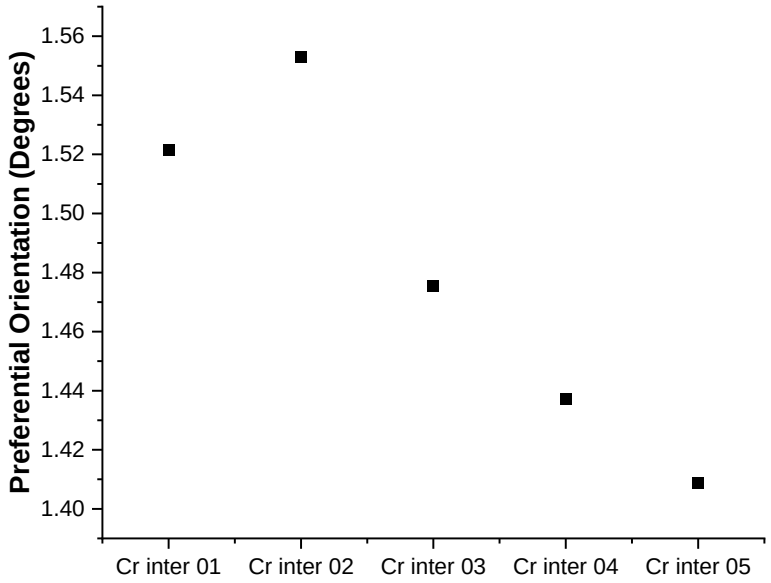

Gph 3. 110 Cr inter peak preferential orientation comparison.

The appreciation of the preferential orientation of the most intense peak in all spectra is shown in the graph 3. Values correspond to Cr film without preferential orientation, i.e., is the value for Cr pattern. As can be seen on the graph 3, the coatings with interlayer decrease the preferential Cr (110) orientation. The interlayer has a negative effect to the (110) preferential orientation during film growth. On the other hand, the samples Cr inter 01 and 02 present higher (110) preferential orientation.

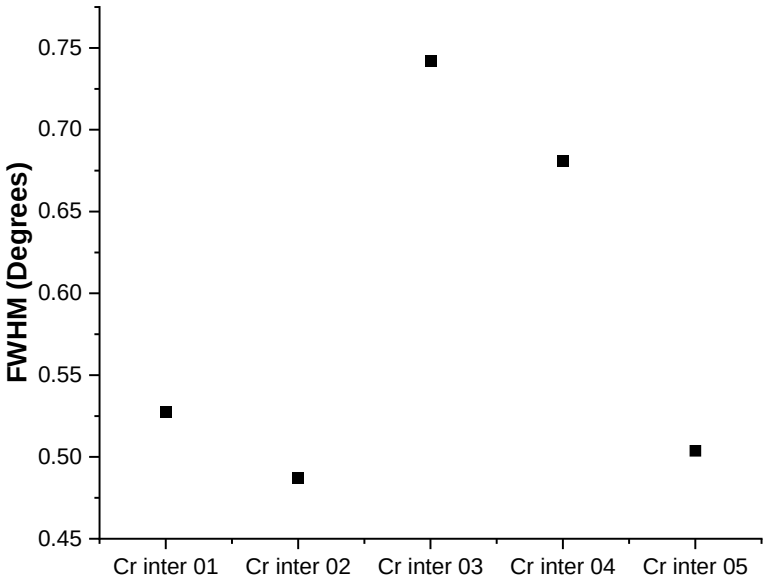

Gph 4. 110 Cr inter peak full width comparison.

The peak width can give some information about possible misalignment of grains, the sharp the peak is the more aligned grains are. In the graph 4 is possible to identify the full width at half maximum of (110) peak for each sample. The Cr inter 03 and 04 are the ones with bigger grain misalignment. The Cr inter 02 has the lower FWHM or best alignment. This can explain the better arrangement of the grains in a particular diffraction pattern. The Cr inter 03, 04 and 05 have similar peak FWHM, meaning that the alignment of the grains is almost equal for those films.

5.1.2. Films Morphology and Composition

As can be seen on the micrographs on the figure 8 obtained by SEM, the morphology of the films is dense and constant with some sort of circumferential features equally distributed in the planar section. The films Cr inter 01, 02 and 04 have no huge defects or porosity visible, and in the cross-view micrographs the column grown characteristic for the pure chromium films is recognizable and constant in all samples.

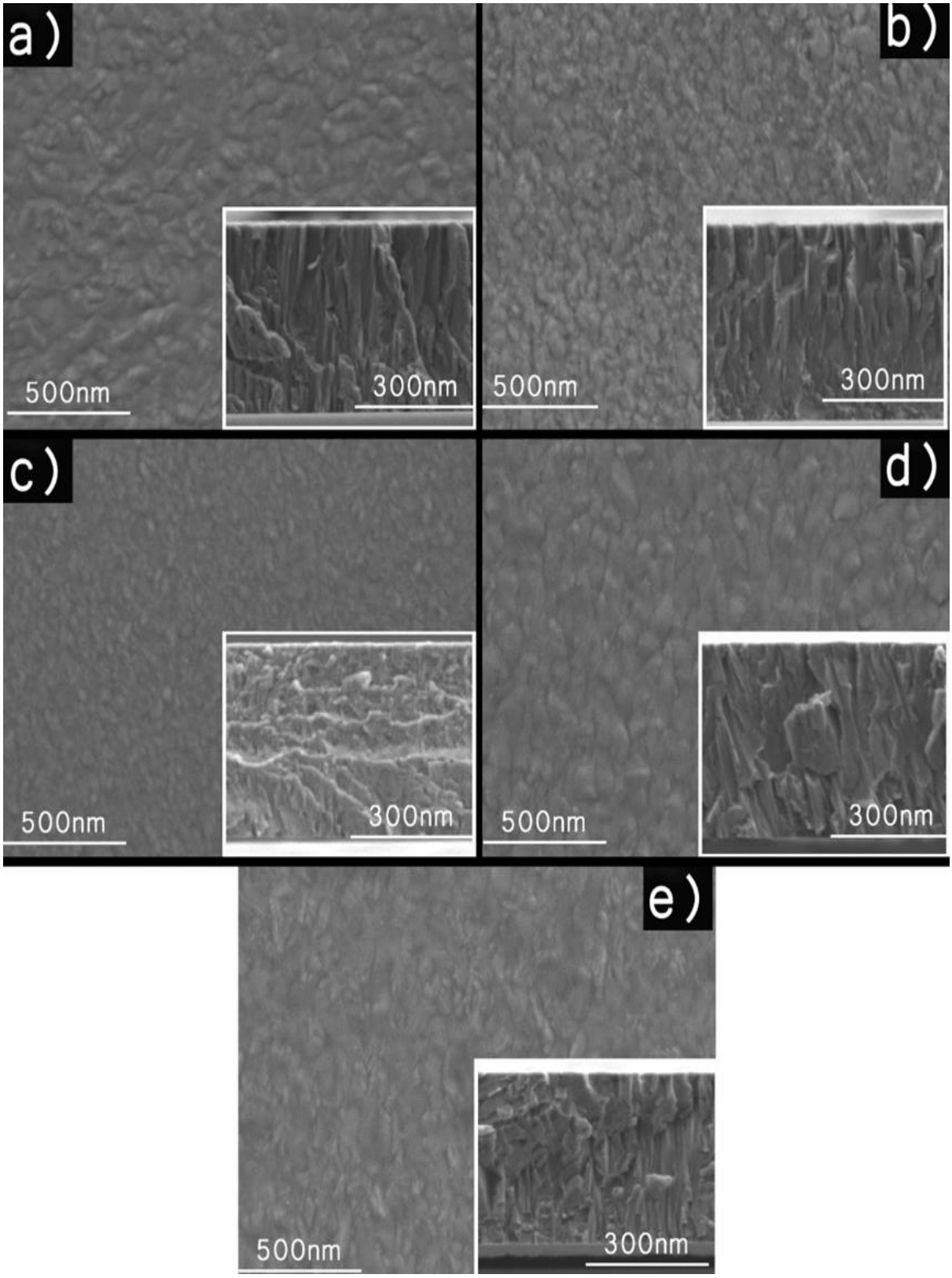

Fig. 8. Films morphology planar view and cross section micrographs for: (a) Cr inter 01, (b) Cr inter 02, (c) Cr inter 03, (d) Cr inter 04, and (e) Cr inter 05.

Tab. 6. Thicknesses measured and roughness results for 2x2 μm scan.

	Interlayer(nm)	Film (nm)	Roughness (nm)
Cr inter 01	x	983	3.0
Cr inter 02	x	1010	3.4
Cr inter 03	119	1119	1.1
Cr inter 04	209	1209	2.9
Cr inter 05	*100*	1016	3.1

From the SEM cross-section micrographs of Fig. 8, some estimation and definition of the films thickness was done, and the values are collected in Table 6. The interlayer was not distinguishable in any circumstances, since both interlayer and film correspond to the same sputtered material, in this particular case chromium. However, since for the Cr film similar conditions and time was used (DOMS 1 μm Cr) it is possible to estimate the film and interlayer thicknesses. On the table 6 is shown that the Cr inter 03 and 04 the end goal of depositing 100 nm and 200 nm was successfully achieved. For the last film, considering Cr inter 01 sample 983 nm, we can estimate approximately 40 nm of interlayer. The interlayer process time estimation was not correct.

The Chromium films roughness was measured by atomic microscopy to verify the systems surface topography variations related with the etching and interlayer used.
On the table 6 is exposed a small summary of the surface roughness for each sample as well. With exception of Cr inter 03 sample, all specimens have similar values around 3 nm. Cr inter 03 has lower surface roughness of 1.1 nm.

5.1.3. Mechanical Film Properties

During the deposition due to high bombarding energy levels, internal residual stresses can arise. These values are important to understand the capability of the film to support and handle high stresses performance conditions. In graph 5 is possible to identify that Cr inter 02 has the highest level of residual stresses, meanwhile the other 4 interlayers share almost the same level presenting lowest values of residual stresses. Cr inter 05 has the lowest value.

For a better understanding and precise comprehension of the film adhesion, scratch test was performed for the specimens. The critical loads of failure (LC) extracted from the

images in Fig. 9 allow to rank Cr films adhesion. The LC values are collected and plotted in Gph 6.

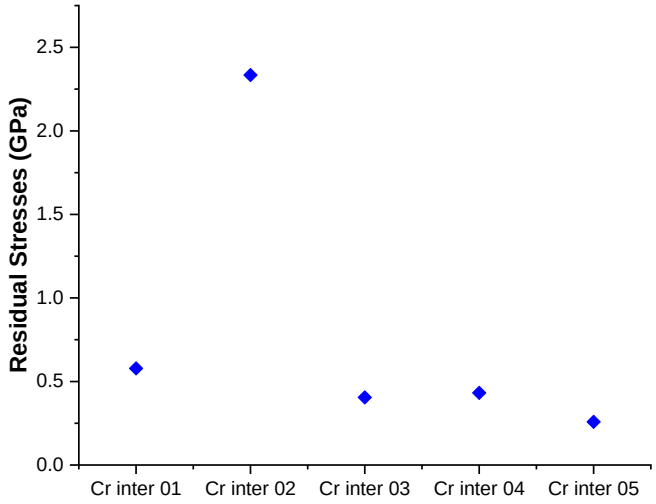

Gph 5. Cr inter samples residual stresses comparison.

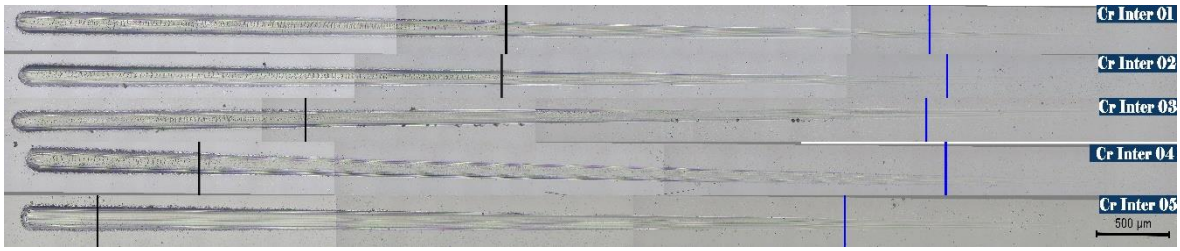

Fig. 9. Scratches test images collected for Cr inter samples. The blue lines correspond to LC1 when minor damage starts and black lines to LC2 which corresponds to higher film damage.

Similar failure behaviour is obtained for the coatings without interlayer, Cr inter 01 and 02. Their LC2 values are 40N for both. On the other hand, the Cr inter 03 and 04 films have LC2 values at 52N and 60N respectively, suggesting higher load support. Finally, Cr inter 05 film has the best behaviour between all the films, with LC2 near 70 N. This is sign that this coating has higher capacity to handle higher forces before failure, when comparing to the other films.

Sample Cr inter 05 according to this test is an interesting candidate for deposition of thicker chromium films.

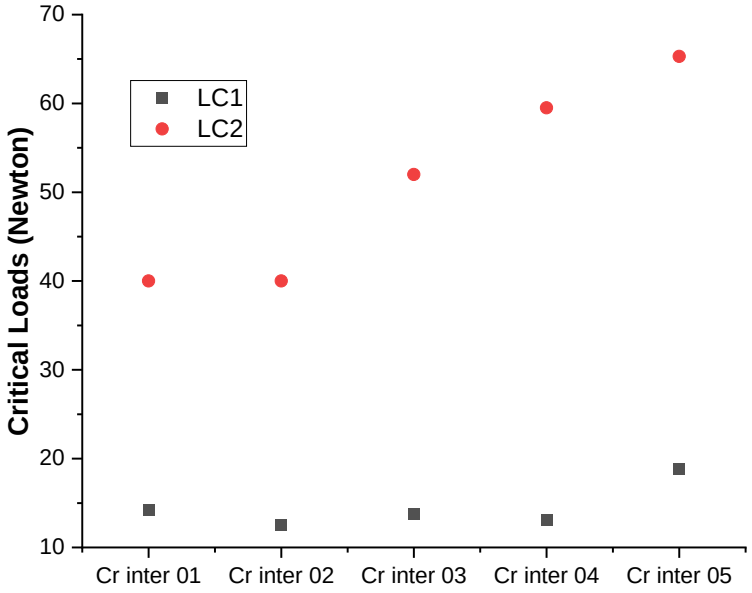

Gph 6. Cr inter samples critical load values collected from scratch test images.

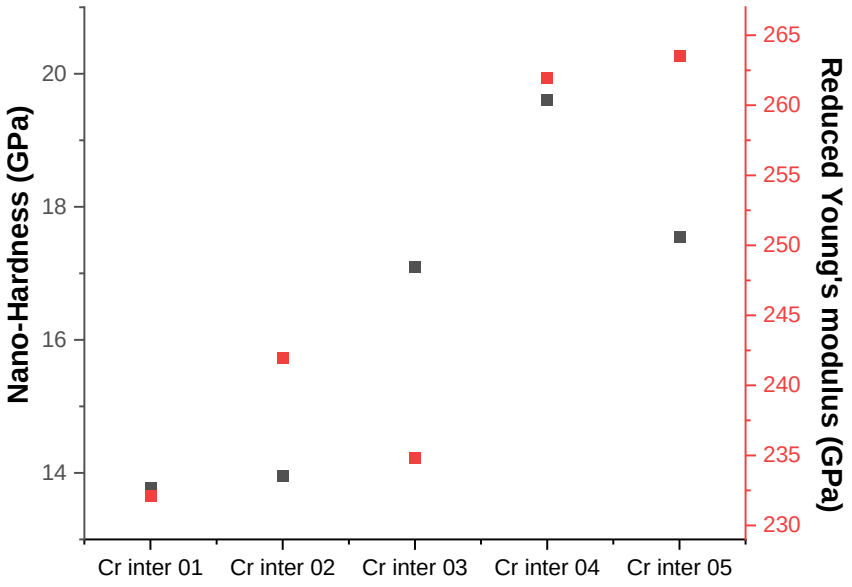

Gph 7. Nano hardness using 5 mN loading and reduced Young's modulus.

On graph 7 the hardness for each sample is compared. The hardness and Young's modulus results can have compromised accuracy since the interaction of the substrate is possible due to the very low thickness, interlayer of a few nanometres plus coating of near 1 micron thickness. The penetration depth measured in the tests was of 120 nm which is enough to calculate the property without significant substrate influence, since this value is less than one seventh of the total film thickness. Nevertheless, the Young's modulus is always affected by the substrate.

Cr inter 01 and Cr inter 02 films hardness is 14 GPa, Cr inter 03 and 05 present 18 GPa, while Cr inter 04 film shows the highest hardness value of 20 GPa. The modulus results follow similar trend like hardness, lower for Cr inter 01 and 02, higher but similar again for Cr inter 03 and 05, and finally with the highest value for Cr inter 04.

At this point of the results, it is possible to establish that Cr inter 04 and 05 have the higher mechanical properties, being the best candidates to take into consideration for the next stage of the project.

5.1.4. Tribological film behaviour

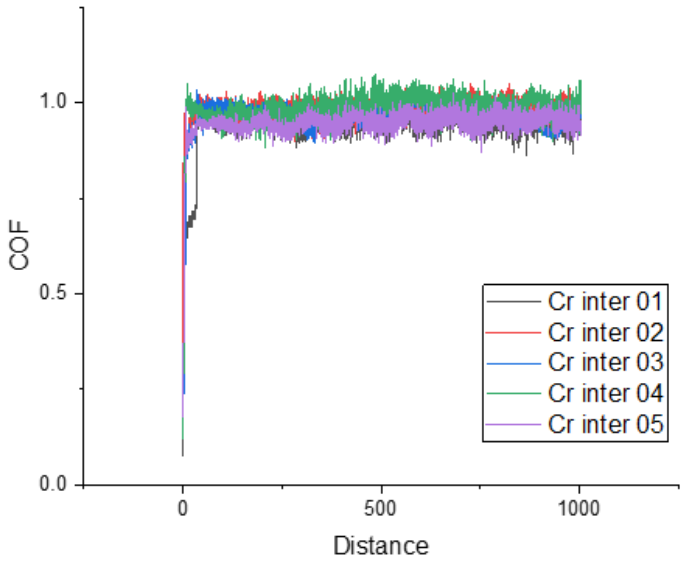

Gph 8. Coefficient of friction for pin-on-disk testes with 3N load of the Cr inter samples.

In the graph 8 is presented the CoF of the Cr inter samples. All show similar CoF value in the range of 1.0, after the initial running-in period (better seen in the magnification of Graph 9).

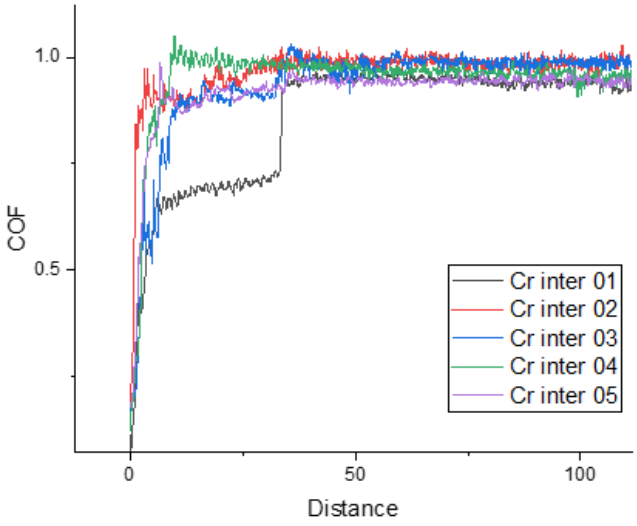

Gph 9. Magnification of graph 9 for first 100 meters.

In the first 100 m of testing running, can be visible the small difference in the samples related with running-in accommodation between sample and ball. The CoF values then stabilize at the same 1.0 value independent of the sample.

In Fig. 10 are the SEM micrographs of the worn tracks after pin-on-disk testing for the Cr inter samples. From the SEM images it is possible to notice that all the samples have wear marks. It can be also seen black areas which correspond to pin debris released and included in the film during the testing. The EDS analysis (Table 7) on these locations help to establish the wear mechanism. The black areas correspond to iron oxide debris transferred from the pin. Their presence during the sliding tests leads to increased wear as they are sling together with the pin and sample surface damaging the coating. The pin debris oxidation also led to difficulties in wear measurement, since the oxidised particle volume is bigger than correspondent reduced form.

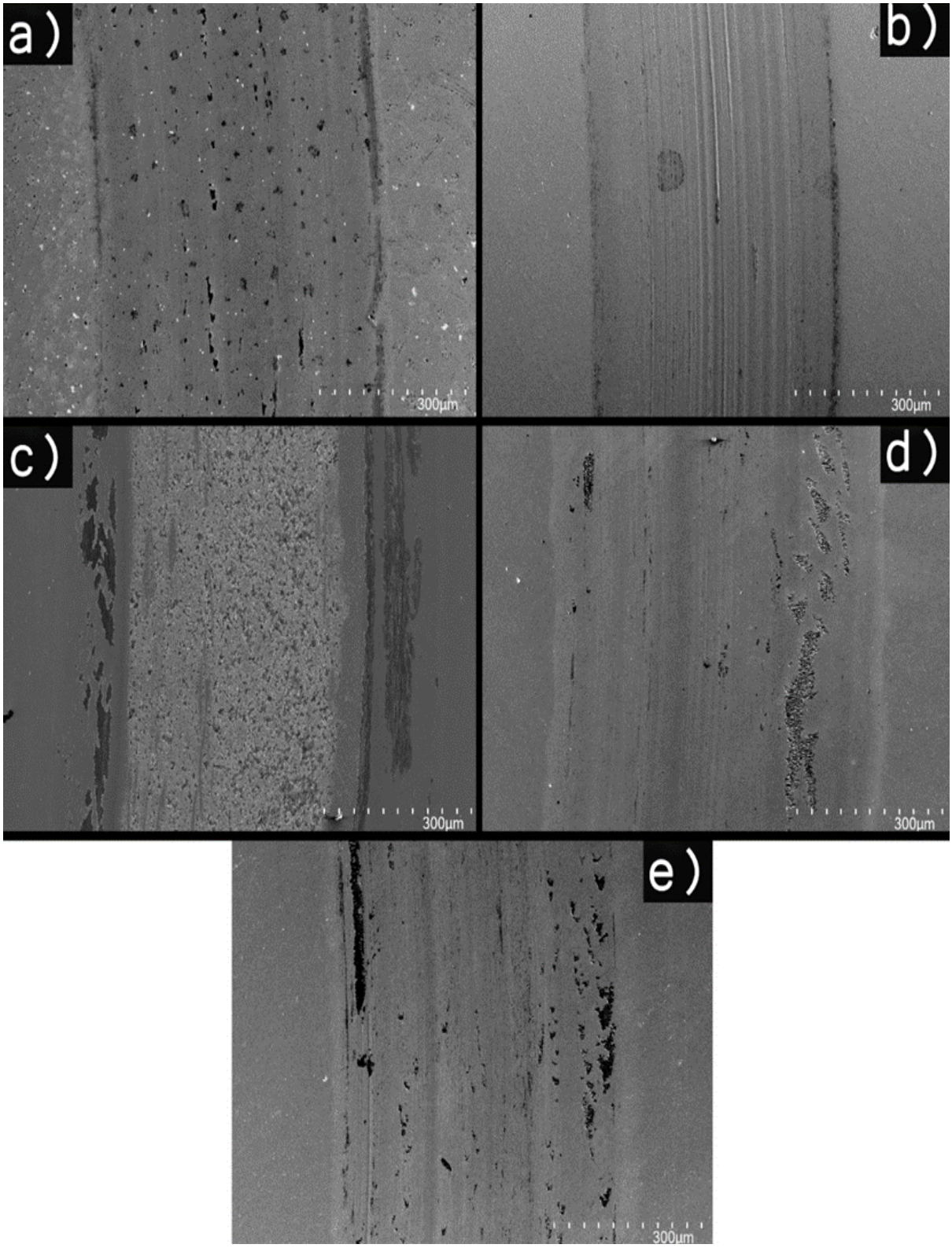

Fig. 10. SEM micrographs of the wear tacks after pin-on-disc testing for: (a) Cr inter 01, (b) Cr inter 02, (c) Cr inter 03, (d) Cr inter 04, and (e) Cr inter 05.

Figure 11 corresponds to SEM micrograph of the Cr inter 03 worn track. Shows the EDS where was performed the analysis, being (1) the wear coating, (2) the pin debris. This image was selected due to its wear damage.

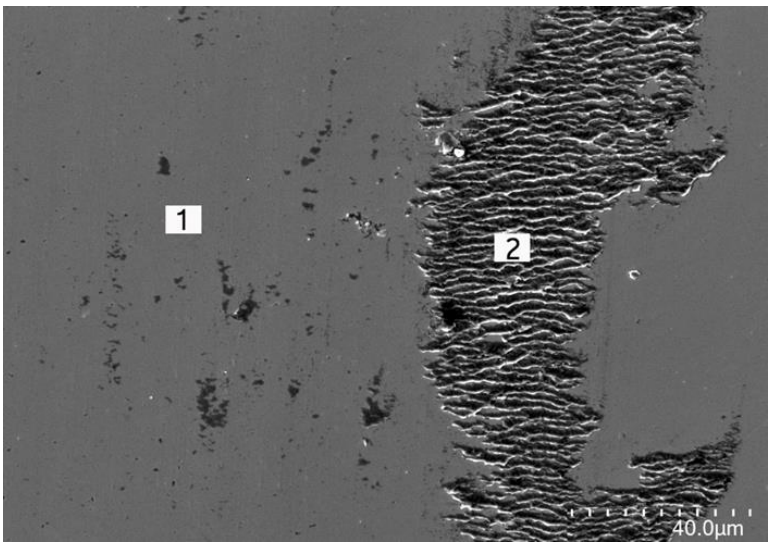

Figure 11. Example of SEM micrograph of worn area after pin-on-disc testing in Cr inter 04 sample, where EDS analysis were performed. Selected zones: 1) Worn coating and 2) pin debris included in the coating.

Tab. 7. Element atomic percentage composition for the Cr inter films and wear tracks from pin-on-disc.

3N	Coating	Worn coating	Pin Debris	Composition
Cr inter 01	95.9	90.1	55.2	Cr
	0.5	5.3	3.3	Fe
	3.6	4.4	41.5	O
Cr inter 02	96.4	95.4	75	Cr
	0.4	1.1	1.2	Fe
	3.2	3.5	23.8	O
Cr inter 03	93.9	94.7	10	Cr
	0.6	0.7	89.9	Fe
	5.6	4.6	0.2	O
Cr inter 04	97.3	92.9	47.1	Cr
	0.4	3.9	2.1	Fe
	2.3	3.2	51	O
Cr inter 05	97	96.4	50.8	Cr
	0.5	0.7	1.7	Fe
	2.5	2.9	47.6	O

In table 7, on the worn coating exist a slightly variation of oxygen and iron, the concentration has increased in an small portion in all samples, meaning that in the dry contact zone exhibit some material transfer and oxidation, even if the coating it is not damaged, the change exists, besides, the concentration of Chromium has decrease as well in the full set of specimens, the material concentration has changed on the contact zone during the test.

From the EDS analysis of the debris, according to the percentages analysed on the surface, it corresponds to iron oxide and chromium oxide, due to the higher levels of oxygen in that zone, confirming the existence of oxidation on the top of the film. Cr inter 03 as it is feasible, this particular sample presents a huge level of iron, suggesting material transfer from the ball.

For the tribological testing, 3-newton load was fixed for further analysis based on several previous trials on these coatings.

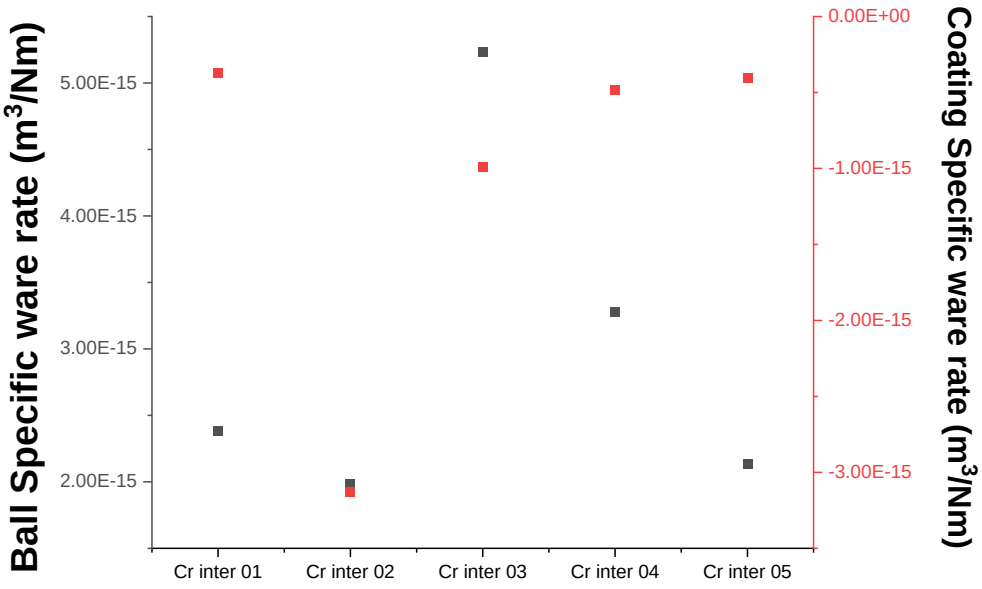

Gph 10. Cr inter samples specific ware rate after pin-on-disk tested with 3 N loads.

In the graph 10, is plotted the specific wear rate of the coating and the ball after pin-on-disk testing with 3N load during 1000 m. Cr inter 01, 04 and 05 possess almost similar loss percentage in the ball and the track with slightly variances. Cr inter 02 has a higher loss

of material, meaning that the coating cannot handle 3 newtons load. As can be noticed Cr inter 05 has the minimum loss of material during the tribological trial, it can handle and perform better wear conditions comparing to the other samples.

5.2. THICKER CHROMIUM FILMS DEVELOPMENT

For the second stage, 4 samples and 2 different thicknesses were used for further characterization. Two samples have 3 microns total thickness, with substrate bias of -60V in the last two microns, and other two samples with 5 microns total thickness, with substrate bias of -60V in the last four microns. One sample of each thickness had the selected interlayer before the Cr film.

5.2.1. Film Structure

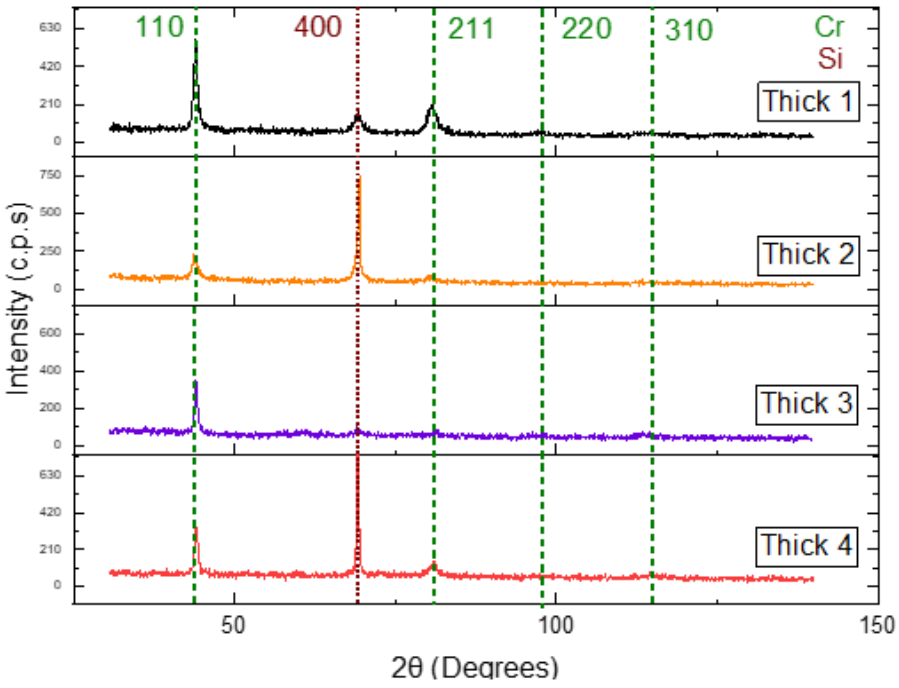

Gph 11. XRD Diffractograms of Cr thick samples.

On the graph 11 are the XRD spectra obtained for Cr thick samples. The peak (110) continues to be the most intense one, like what was previously obtained for Cr inter samples. In this case, there is also development of (211) peak in some samples. The (400) silicon substrate corresponding peak is also visible.

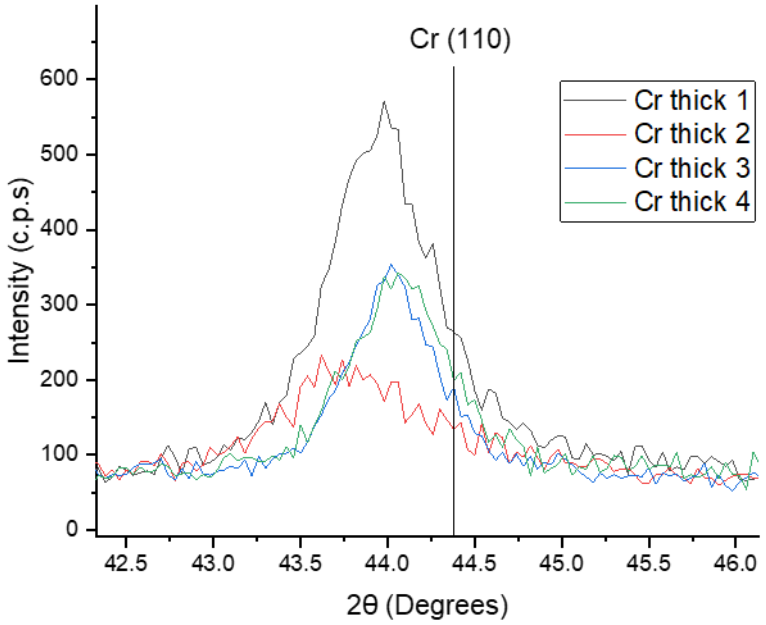

Gph 12. Cr thick Chromium peak (110) diffractogram comparison.

In Graph 12 are high resolution XRD scans performed in (110) and (211) regions for Cr thick samples. The results present a clear peak shifting for all samples comparing with the Cr peak position patter for pure chromium (ICDD 00-006-0694). Samples deposited without interlayer, Cr thick 1 and 4, present higher intensity comparing to the ones with interlayer, Cr thick 2 and 3. Nevertheless, all peaks have lower intensity compared to the previous stage samples. Peak shifting to the left in the spectra is still observed. The Cr thick 1 has the highest intensity. The graph 12 indicates that the interlayer samples have wider and less intense peaks in the spectra in this set of samples.

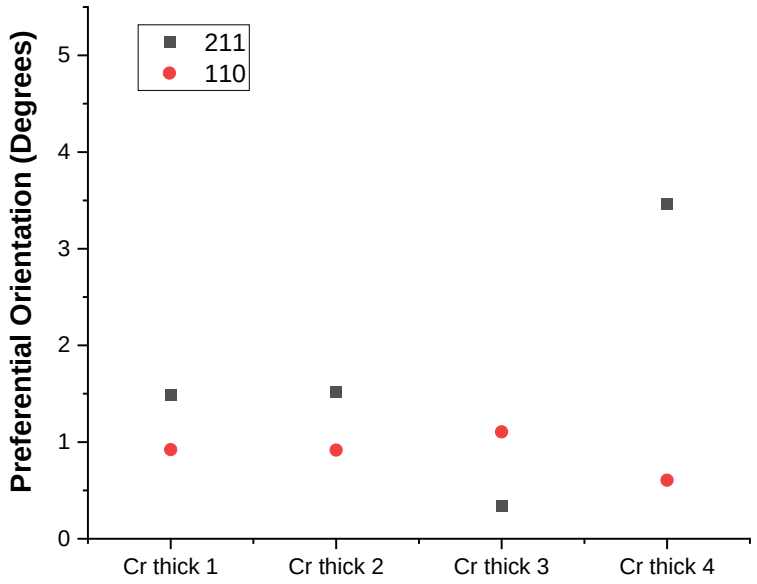

Gph 13. 110 and 211 Cr thick peaks preferential orientation comparison.

In the graph 13 are the preferential orientation for the Cr thick samples. The coatings with interlayer have a slightly increase of the preferential Cr (110) orientation, meanwhile the samples without interlayer already have preferential orientation for the Cr (211) peak. Cr thick 1, 2 and 4 are oriented in the Cr (211) plan.

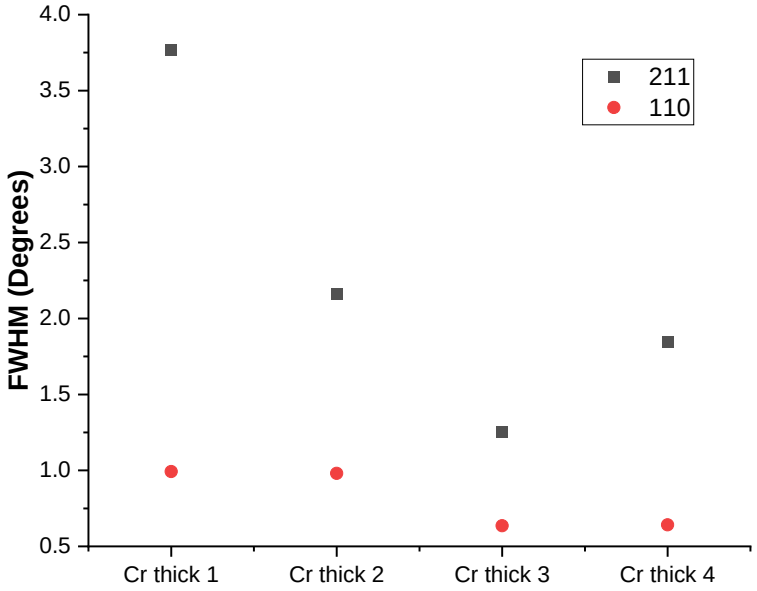

Gph 14. 110 Cr thick peak full width comparison.

In the graph 14 is the full width at half maximum for Cr (110) and (211) for the Cr thick samples. The samples with interlayer, exhibit closer grain alignment to the pattern, regardless of the thickness. However, higher thickness higher arrangement regardless of the interlayer. Cr thick 1 presents bigger misalignment in both peaks, while Cr thick 3 has the lower value for both, this can explain a better arrangement of the planes in a particular diffraction pattern.

5.2.2. Film Morphology

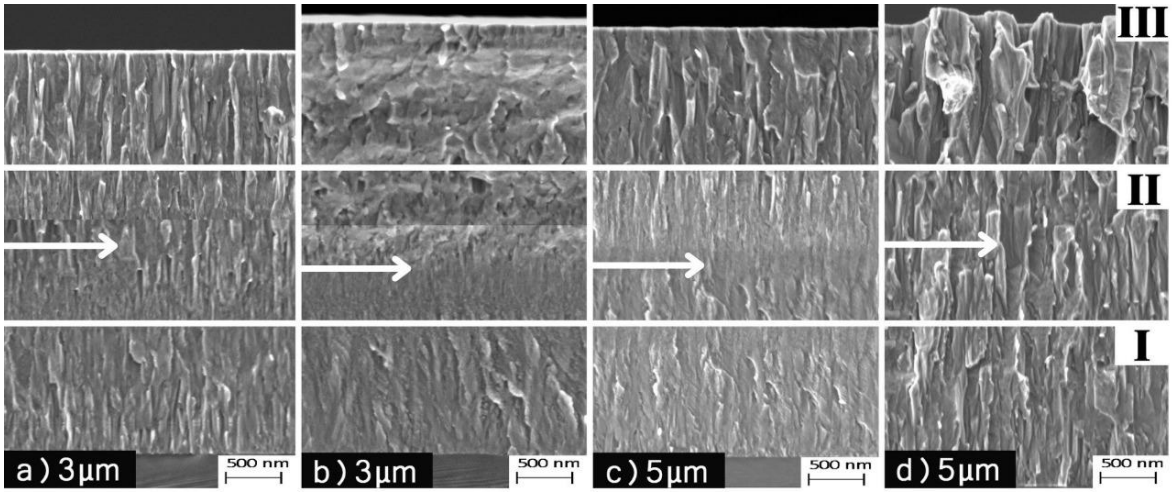

Figure 12. Cross-sectional SEM micrographs of the Cr films deposited by HiPIMS, performed at similar thicknesses. Level I – Next to the substrate, level II – Beginning of bias; level III – film top part, for: (a) Cr thick 1, (b) Cr thick 2, (c) Cr thick 3 and (d) Cr thick 4.

In the figure 12, are present the cross-sectional SEM micrographs, that shows some changes along the film grow. The specimens exhibit a clear substrate polarization ignition during the deposition, but the line is more feasible in the samples with interlayer. The level one seems to be more organized and its visible the characteristic column growth, while in the level three of the same films, the structure shows more density, seem to be more condense on this section.

In the thicker films, Cr thick 1 and 4 applying the substrate bias, the behaviour of the column growth of the coating is much straight and visible. Cr thick 1 and 4 seem to be better distributed and continuously along the cross-section comparing with the interlayer samples.

Moreover, the polarization ignition is not evident in Cr thick 1 and 4, comparing to the interlayer samples, there is no such appreciation or clear evidence of a separate zone across the film growth.

Tab. 8. Thickness measured for Cr thick samples.

	Interlayer (nm)	Film (µm)
Cr thick 1	x	2.4
Cr thick 2	*100*	2.3
Cr thick 3	*100*	4.5
Cr thick 4	x	4.5

Using cross-section SEM micrographs was possible to measure the Cr films thickness, the results are in table 8. Like in the sample of stage one, the interlayer is not discernible making it impossible to measure. The interlayer and the film are made of the same material showing no contrast difference when analysed by SEM.

In figure 13 for better surfaces morphology analysis, the SEM and AFM images micrographs were place together. The SEM micrographs exhibit some small variances depending on the samples thickness. The Cr thick 1 and 2, the 3 µm samples, have undefined surface, like the surface obtained in Cr inter stage, figure 13 (a and b respectively). The thicker samples, Cr thick 3 and 4 figure 13 (c and respectively), on the other hand, have already started to develop defined surface features – surface elongated lines. These features are characteristic effect of growth under the effects of high shadow effects.

From the AFM pictures, the thinner films present lower height comparing to the thicker ones, increase of roughness, which is related with increase of surface features as a result of film increase of thickness.

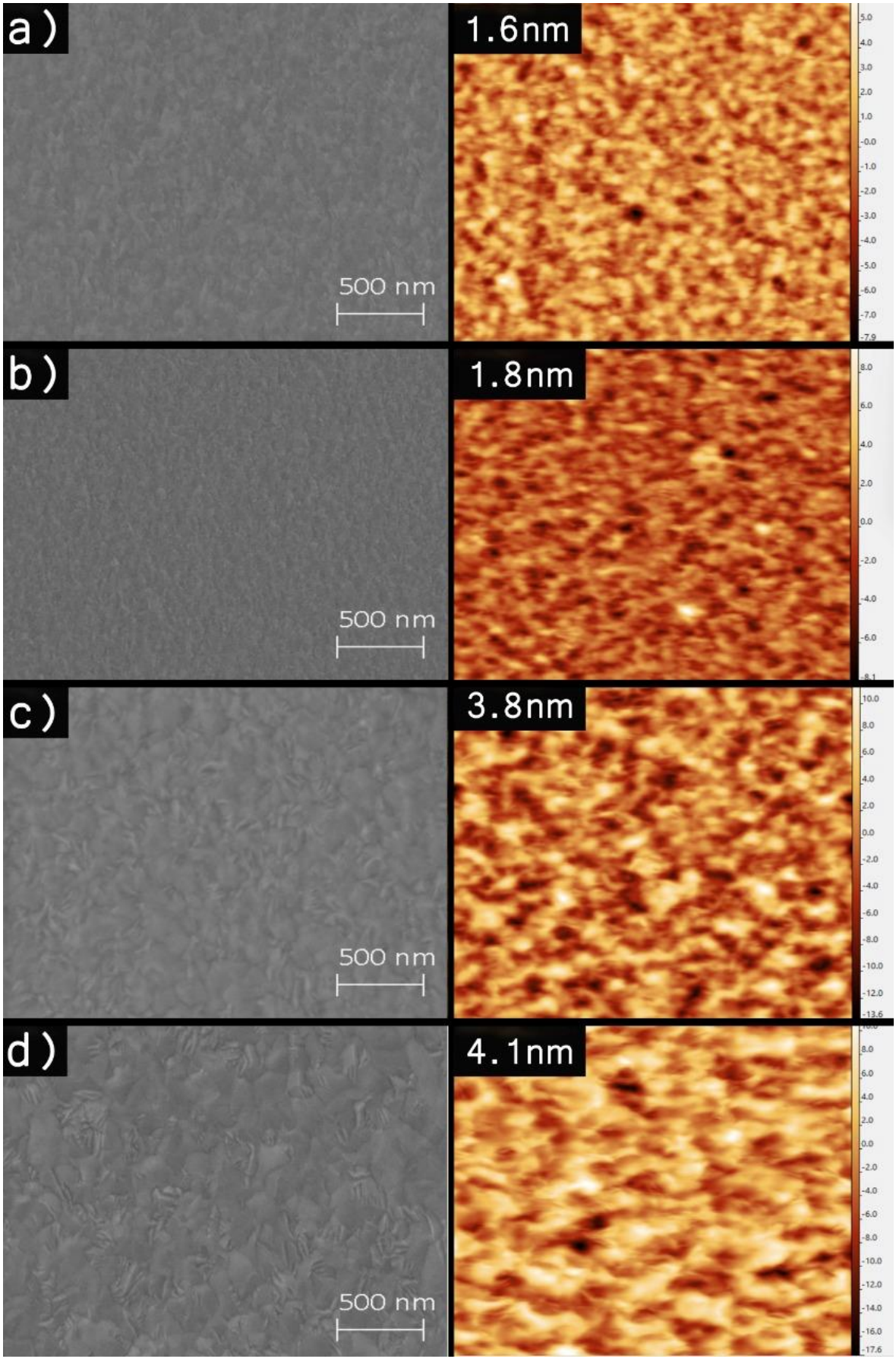
a)
500 nm
1.6nm
b)
500 nm
1.8nm
c)
500 nm
3.8nm
d)
500 nm
4.1nm

Figure 13. SEM micrograph and AFM 4×4 μm scan of the samples surface morphology, for: a) Cr thick 1, b) Cr thick 2, c) Cr thick 3, and d) Cr thick 4. The AFM surface roughness are presented in the respective images.

5.2.3. Mechanical Behaviour

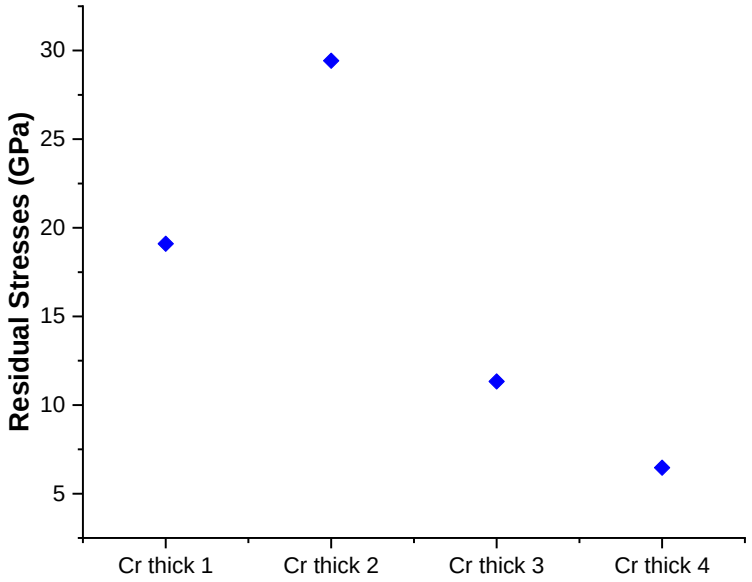

Gph 15. Cr thick samples residual stresses results.

Graph 15 shows the internal residual stress of the Cr thick films. Cr films with interlayer, samples Cr thick 2 and 3 possess higher internal residual stresses when compared with respective samples without the interlayer. The increase of thickness leads to some reduction of internal residual stress for these films.

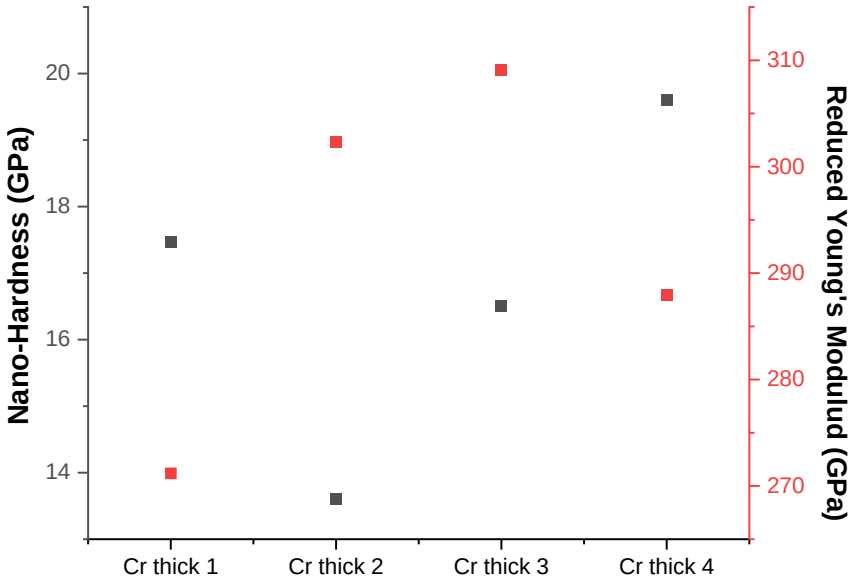

Gph 16. Nano hardness for 20 mN loading and reduced Young's modulus.

Graph 16 shows the hardness and reduced Young's modulus results obtained for Cr thick samples. The hardness results in this set of samples are higher than similar thickness samples developed in past investigation.[47] Here lower value is near 14 Gpa, compared with 12 GPa previously obtained. Sample Cr thick 4 reaches 20 GPa. In the set of samples here presented, Cr thick samples with interlayer present lower hardness values when compared with respective counter sample without interlayer, independent of the thickness.

Regarding the elastic behaviour on the thicker films the substrate influence is less expected since the thicknesses are higher comparing to the previous set of samples. The reduced Young's modulus results of Cr thick 2 and 3 samples have higher values, while Cr thick 1 sample shows is the lowest. It is the possible to conclude that the interlayer enhances the elastic behaviour, probably due to the compactness of this coatings, however, compromises the hardness of the film.

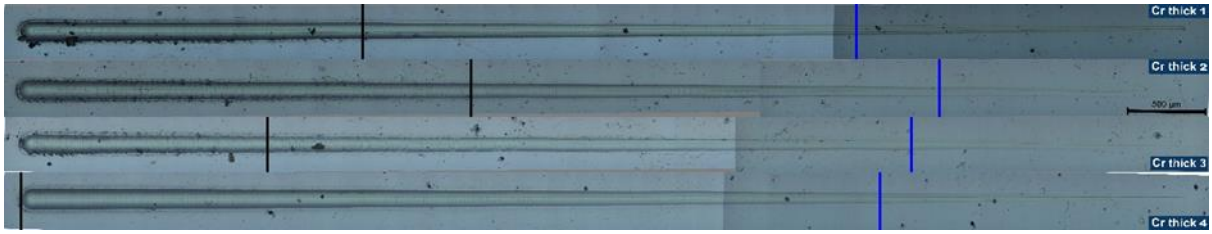

Fig. 14. Scratches results for Cr thick samples. Blue line corresponds to minor damage (LC1) and black line to high cracks or major defects (LC2).

In Figure 14 are the optical images of the Cr thick samples after scratch testing. The different failure modes are marked with blue and black lines for minor damage (LC1) and high cracks or major defects (LC2), respectively. The four samples present similarities with the results obtained in the first stage, Figure 9. The Cr thick films response with increasing load is similar when analysing LC1 failure but significantly different for LC2.failure.

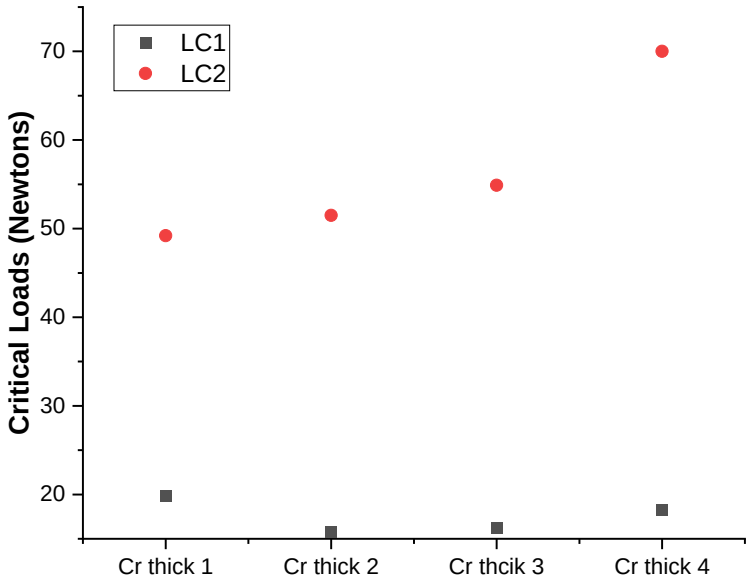

Gph 17. All Cr thick samples critical load on the scratch test comparison.

In graph 17 shows the critical loads of every sample. The LC1 for each specimen is very close, around 19N, while LC2 depends on the Cr film. The Cr thick films without interlayer, present a higher levels load handle, being Cr thick 4 the sample that do not even present LC2, this coating can easily handle 70N. For LC2 the other samples have similar values of around 55N. The influence of the interlayer is not remarkable for the actual adhesion of the thicker films.

5.2.4. Tribological Behaviour

The tribological behaviour of the Cr thick used the same parameters already used for the interlayer development.

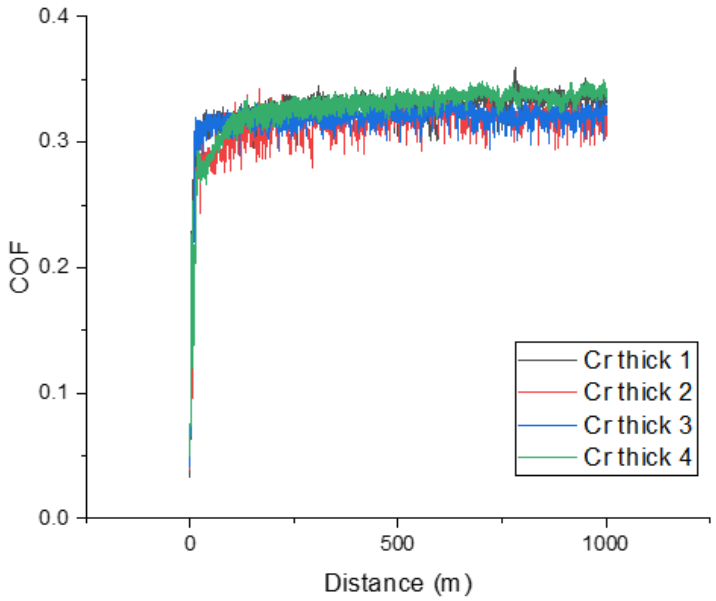

Gph 18. Cr thick CoF during pin-on-disk testing with 3N load.

The graph 18 shows the CoF results for the Cr thick samples. The CoF for the samples are similar about 0.3. The running-in period, shown in graph 19, shows that all samples converged to stable COF behaviour during initial 100 m of pin-on-disk tests.

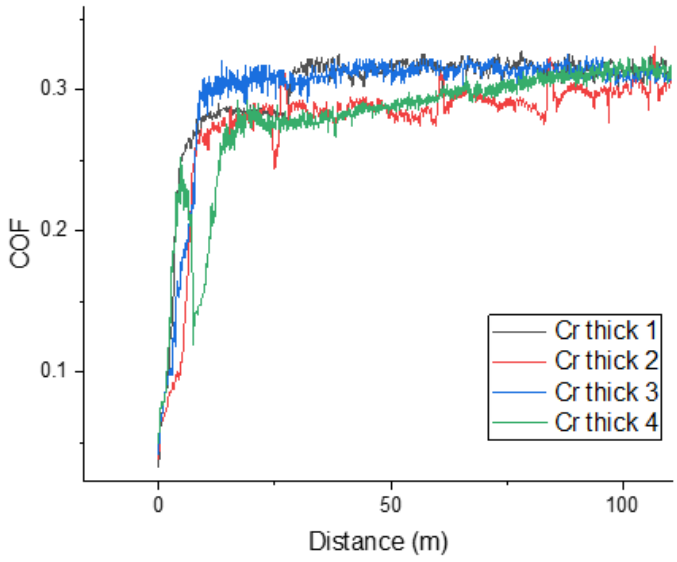

Gph 19. Magnification of graph 19 for initial 100 meters.

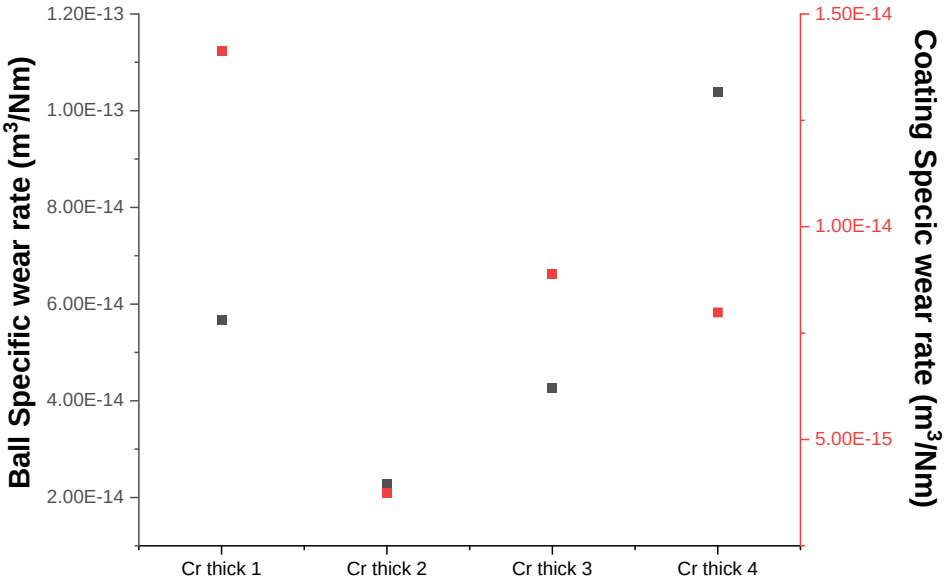

Gph 20. Specific wear rate for 3 newton loads.

On the graph 20 are the specific wear results for the Cr thick samples. The ball worn mark of Cr thick 2 shows the highest loss of material during the experiment. This can be also seen on the SEM micrograph of fig 15a. Cr thick 4 sample has shown better resistance and lower ware rate. This is also the coating that has better performance in the scratch test, supporting up to 70N load without major failure.

Figure 15 shows SEM and EDS characterization made in coatings wear track and in ball worn area.

The wear tracks micrographs exhibit some black areas along the track in all samples except in Cr thick 4 sample.

Regarding the ball marks, Cr thick 2 has bigger worn mark diameter, as it can be also confirmed on the graph 20. The pictures also reveal that film Cr thick 4 ball mark has the smaller diameter.

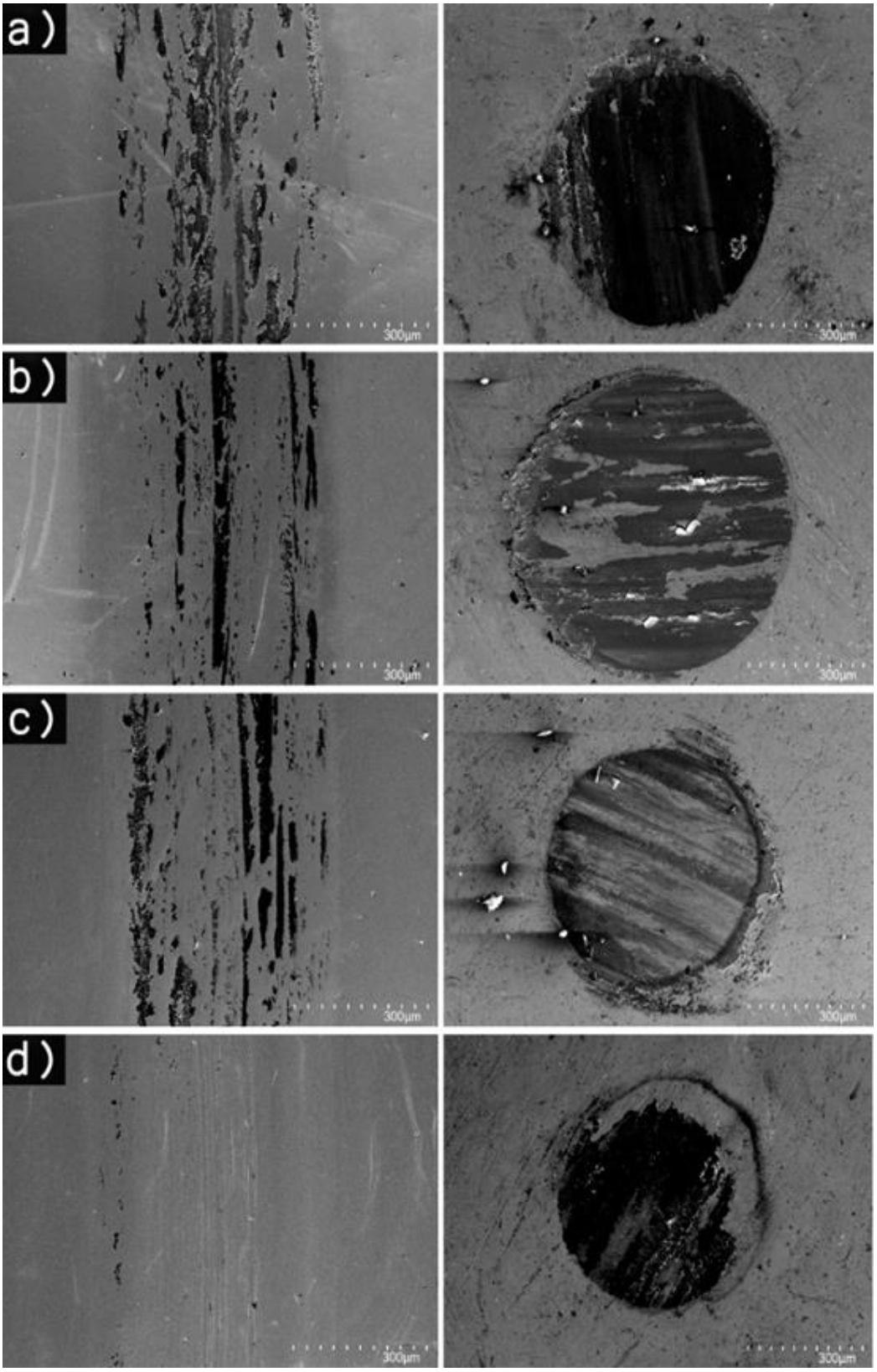

Figure 15. SEM micrographs of the wear tacks and ball worn area for: (a) Cr thick 1, (b) Cr thick 2, (c) Cr thick 3 and (d) Cr thick 4.

EDS chemical composition characterization was performed to clarify what are the different seen zones.

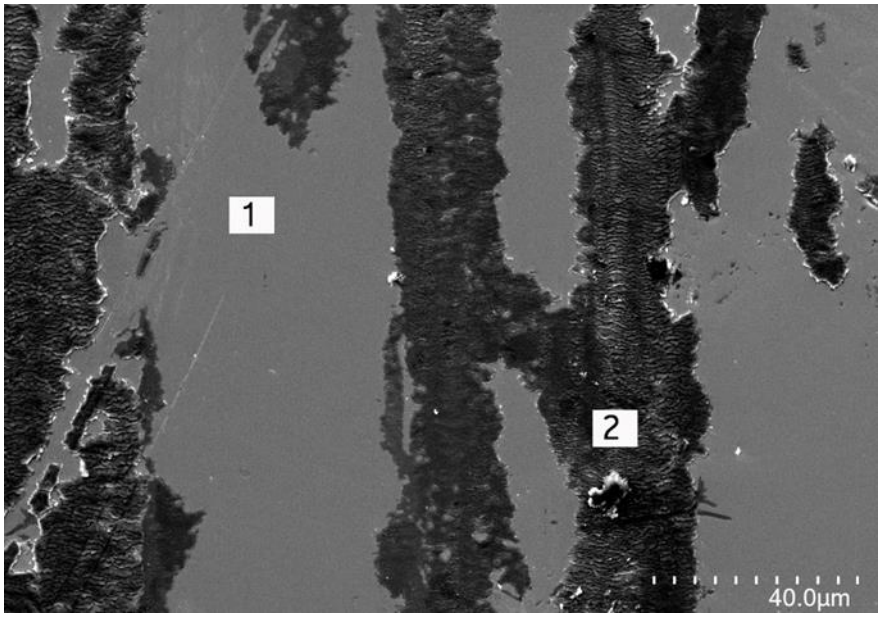

Figure 16. Planar surface section SEM micrograph of the wear tack obtained by Pin-on-disc in the Cr thick 1 for EDS analysis focused on the selected zones.

One image has been chosen to show how was done the EDS on the other films, as can be seen on the figure 16, the data was collected from different zones of the specimen surface, from the black lines which presumably corresponds to ball debris or material transfer from the ball during the experiment, and also the coating itself to actually manifest any variance in the composition in this wear area.

Tab. 9. Element atomic percentage composition present on all Cr thick films, ball debris and wear balls for each sample.

3N	Coating	Worn coating	Pin Debris	Ball	Worn ball	Composition
Cr thick 1	99.3	98.4	33.8	8.5	18.2	Cr
	0	0	5.1	63.2	14.9	Fe
	0.7	1.6	61.1	28.3	66.9	O
Cr thick 2	98.7	97.4	50.2	2.3	20.1	Cr
	0	0	6.8	97.7	7.1	Fe
	1.3	2.7	43.1	0	72.8	O
Cr thick 3	98.1	97.9	49.8	4.4	13.2	Cr
	0	0	2.8	86.7	42.8	Fe
	1.9	2.1	47.4	8.8	44.1	O
Cr thick 4	98.5	97.7	53.9	1.7	22.1	Cr
	0	0	1.8	97.7	6.4	Fe
	1.5	2.4	44.3	0.6	71.6	O

In table 9, is possible to see that iron is null, indication that the influence of the substrate disappears with the increase of thickness. However, on the surface debris iron is obtained, meaning that some ball material transfer occurred during the test. Moreover, oxygen level also increases on the surface debris suggesting material oxidation.

The ball worn areas also present a significant increase of oxygen in its composition, again showing oxidation. Increase of Cr also is measured suggesting that Cr film material is also transferred to the ball during the tests.

6. CHAPTER 6

6.1. Discussion

Throughout the whole project to enhance the adhesion and maintain or increase the tribo-mechanical properties of thick films has been the principal goal, two stages were carried out for this investigation.

For the interlayer development, based on the results obtained, it was possible to analyse the influence of the interlayer in adhesion, mechanical and tribological behaviour of 5 different samples of 1 micron thickness with differences in the interlayer thickness and deposition mode. The film with interlayer of 100 nm deposited with DOMS known, labelled as Cr inter 05, was selected for further analysis as thicker chromium films.

On the thicker chromium films development, the influence of the interlayer and substrate bias implementation was analysed, mainly focusing on the impact of the deposition conditions of film increased density. On this part the focal point was the development of thicker, dense chromium films, to identify the real importance and utility of the interlayer. On the thicker film development, 3-micron and 5-micron thicknesses were analysed, with and without interlayer and with substrate bias.

Based on the results obtained, it has been proved that the interlayer has a small influence on the adhesion and tribological properties but significant influence in the mechanical properties. The substrate bias, on the other hand, showed a significant increase in the tribological and mechanical properties when compared with previously developed coatings without bias.

6.2. Conclusions

1. Performing the pin-on-disc tests, the coefficient of friction of the thick films decreases. From Cr inter samples 1.0 CoF to Cr thick samples 0.3.

2. Interlayers are not recommended to maintain preferential orientation growth and therefore the structure may change for thicker films.

3. In one micron films the presence of iron is feasible, substrate influence, while for thicker films it does not appear.

4. Interlayer enhances the hardness and adhesion of the films, nevertheless, compromises other properties.

5. The interlayer is an improvement, but it has been shown that the deposition with bias and without interlayer present visible differences in the properties of thicker Chromium films.

6. The substrate bias tends to decrease the shadowing effect giving different mechanical characteristics to the coatings.

7. With substrate bias the coatings seem to be denser, showing better tribo-mechanical performance.

8. Iron balls are inefficient to be accurate in the wear resistance for the achieved coatings.

6.3. Recommendations

- Harder material balls for wear conditions to be able to calculate accurately the wear resistance since Iron balls are considerable losing material on the Chromium coatings.
- Use lower bias voltage for depositing Chromium films since 60 volts can less influence the silicon samples.
- Scratch testing can use higher load since the coatings already handle 70 newtons without major failure.
- To densify the coating the bias can be turn on in different film sections, to densify the Cr films at different zones. Densification near the surface or closer to the substrate can provide differences in adhesion or wear resistance in the thicker films.

BIBLIOGRAPHY

[1] Krishna. Seshan. (2002). "*Handbook of thin-film deposition processes and techniques: principles, methods, equipment and applications"*. Noyes Publications.

[2] D. M. Mattox. (1998). "*Handbook of physical vapor deposition (PVD) processing: film formation, adhesion, surface preparation and contamination control"*. Noyes Publications.

[3] D. Depla, S. Mahieu, and J. E. Greene. (2010). "*Sputter Deposition Processes*," in *Handbook of Deposition Technologies for Films and Coatings*, Elsevier Inc. pp. 253–296. doi: 10.1016/B978-0-8155-2031-3.00005-3.

[4] P. Brault. (2004). *"Plasma sputtering deposition of platinum into porous fuel cell electrodes," Journal of Physics D: Applied Physics*, vol. 37, no. 24, pp. 3419–3423.

[5] R. S. Rastogi and K. Pourrezaei. (1994). *"Deposition, characterization, thermo-chemical compatibility and failure analysis of multi-layer coated silicon-carbide fibre-reinforced metal-matrix composites".*

[6] R. Keshavamurthy, M. Sudhan, A. Kumar, V. Ranjan, P. Singh, and A. Singh. (2018). *"Wear Behaviour of Hard Chrome and Tungsten Carbide-HVOF Coatings".*

[7] A. Gossart. (2019). "*Coating of cobalt chrome substrates with thin films of polar/hydrophobic/ionic polyurethanes: Characterization and interaction with human immunoglobulin G and fibronectin*". *Colloids and Surfaces B: Biointerfaces*, vol. 179, pp. 114–120.

[8] M. Fröhlich, R. Braun, and C. Leyens. (2006). "*Oxidation resistant coatings in combination with thermal barrier coatings on γ-TiAl alloys for high temperature applications*," *Surface and Coatings Technology*, vol. 201. pp. 3911–3917.

[9] V. Teixeira. (2001). *"Spectrally selective composite coatings of CrCr O and 2 3 MoAl O for solar energy applications"*.

[10] B. Bhushan, G. S. A. M. Theunissen, and X. Li. (1997). *"Tribological studies of chromium oxide films for magnetic recording applications"*.

[11] A. Ghailane, M. Makha, H. Larhlimi, and J. Alami. (2020). "*Design of hard coatings deposited by HiPIMS and dcMS,*" *Materials Letters*, vol. 280.

[12] D. Ludin, T. Minea, and J. Gudmundsson. (2019). "*High Power Impulse Magnetron Sputtering."*

[13] J. T. Gudmundsson. (2010). "*The high-power impulse magnetron sputtering discharge as an ionized physical vapor deposition tool in Vacuum"*, vol. 84, no. 12, pp. 1360–1364.

[14] U. Helmersson, M. Lattemann, J. Bohlmark, A. P. Ehiasarian, and J. T. Gudmundsson. (2006). *"Ionized physical vapor deposition (IPVD): A review of technology and applications*" *Thin Solid Films*, vol. 513, no. 1–2. pp. 1–24.

[15] J. T. Gudmundsson, N. Brenning, D. Lundin, and U. Helmersson. (2012). "*High power impulse magnetron sputtering discharge*". *Journal of Vacuum Science & Technology A: Vacuum, Surfaces, and Films*, vol. 30, no. 3, p. 030801.

[16] N. Britun, T. Minea, S. Konstantinidis, and R. Snyders. (2014). "*Plasma diagnostics for understanding the plasma-surface interaction in HiPIMS discharge*". Journal of Physics D: Applied Physics, vol. 47, no. 22.

[17] S. M. Meier, A. Hecimovic, T. v. Tsankov, D. Luggenhölscher, and U. Czarnetzki. (2018). "*First measurements of the temporal evolution of the plasma density in HiPIMS discharges using THz time domain spectroscopy*". Plasma Sources Science and Technology, vol. 27, no. 3.

[18] V. Tiron, I. L. Velicu, D. Cristea, N. Lupu, G. Stoian, and D. Munteanu. (2018). *"Influence of ion-to-neutral flux ratio on the mechanical and tribological properties of TiN coatings deposited by HiPIMS".* Surface and Coatings Technology, vol. 352, pp. 690–698.

[19] H. M. Urbassek and J. Michl. (1987). "*A gas-flow model for the sputtering of condensed*".

[20] B. Window. (1995). "*Recent advances in sputtering deposition*". Surface and Coatings technologies, vol 71, pp 93-97.

[21] M. Aggerbeck, A. Junker-Holst, D. V. Nielsen, V. C. Gudla, and R. Ambat. (2014). "*Anodisation of sputter deposited aluminium-titanium coatings: Effect of microstructure on optical characteristics*". Surface and Coatings Technology, vol. 254, pp. 138–144.

[22] Mattox, D. M. (1999). Physical vapor deposition (PVD) processes. Metal Finishing, 97(1), 417-430.

[23] J. E. Pawel, C. J. Mchargue, and J. J. Wert. (1990). *"The influence of ion bombardment on the adhesion of thin films to substrates".*

[24] J. A. Thornton. (1977). "*The influence of bias sputter parameters on thick copper coatings deposited using a hollow cathode*".

[25] P. Le. (2017). "*Programmable chiral nanocolloids*". Ecole polytechnique fédérale de lausanne.

[26] P. Panjan, M. Čekada, M. Panjan, and D. Kek-Merl. (2009) "*Growth defects in PVD hard coatings*". Vacuum, vol. 84, no. 1, pp. 209–214.

[27] P. Panjan, D. Kek Merl, F. Zupanič, M. Čekada, and M. Panjan. (2008). "*SEM study of defects in PVD hard coatings using focused ion beam milling*". Surface and Coatings Technology, vol. 202, no. 11, pp. 2302–2305.

[28] H. B. Profijt, P. Kudlacek, M. C. M. van de Sanden, and W. M. M. Kessels. (2011). "*Ion and Photon Surface Interaction during Remote Plasma ALD of Metal Oxides*". Journal of The Electrochemical Society, vol. 158, no. 4, p. G88.

[29] K. Shin. (1992). "*Technologies for enhancing multi-gate Si MOSFET performance".*

[30] Y. Oka, M. Kirinuki, Y. Nishimura, K. Azuma, E. Fujiwara, and M. Yatsuzuka. (2004). "*Measurement of residual stress in DLC films prepared by plasma-based ion implantation and deposition".* Surface and Coatings Technology, vol. 186, no. 1-2 SPEC. ISS., pp. 141–145.

[31] R. Daniel, K. J. Martinschitz, J. Keckes, and C. Mitterer. (2010). "*The origin of stresses in magnetron-sputtered thin films with zone T structures*". Acta Materialia, vol. 58, no. 7, pp. 2621–2633.

[32] R. P. B. Viloan, U. Helmersson, and D. Lundin. (2021). "*Copper thin films deposited using different ion acceleration strategies in HiPIMS*". Surface and Coatings Technology, vol. 422.

[33] G. Greczynski. (2014). "*A review of metal-ion-flux-controlled growth of metastable TiAlN by HIPIMS/DCMS co-sputtering*". Surface and Coatings Technology, vol. 257, pp. 15–25.

[34] S. Gauter, M. Fröhlich, W. Garkas, M. Polak, and H. Kersten. (2017). *"Calorimetric probe measurements for a high voltage pulsed substrate (PBII) in a HiPIMS process*". Plasma Sources Science and Technology, vol. 26, no. 6.

[35] K. GracePavithra, V. Jaikumar, P. S. Kumar, and P. S. SundarRajan. (2019*). "A review on cleaner strategies for chromium industrial wastewater: Present research and future perspective*". Journal of Cleaner Production, vol. 228.

[36] E. V. S. Hessel, Y. C. M. Staal, A. H. Piersma, S. P. den Braver-Sewradj, and J. Ezendam. (2021). "*Occupational exposure to hexavalent chromium. Part I. Hazard assessment of non-cancer health effects".* Regulatory Toxicology and Pharmacology, vol. 126.

[37] H. Oliveira. (2012). "Chromium as an Environmental Pollutant: Insights on Induced Plant Toxicity," Journal of Botany, vol. 2012, pp. 1–8.

[38] M. Gochfeld and C. Witmerft. (1991). "*A Research Agenda for Environmental Health Aspects of Chromium*".

[39] A. K. Shanker, C. Cervantes, H. Loza-Tavera, and S. Avudainayagam. (2005). *"Chromium toxicity in plants*". Environment International, vol. 31, no. 5.

[40] H. Nigam. (2015). "*Effect of chromium generated by solid waste of tannery and microbial degradation of chromium to reduce its toxicity*".

[41] M. Yoshinaga. (2018). *"A comprehensive study including monitoring, assessment of health effects and development of a remediation method for chromium pollution*". Chemosphere, vol. 201, pp. 667–675.

[42] A. Bielicka, I. Bojanowska, and A. Wiśniewski. (2005). *"Two Faces of Chromium-Pollutant and Bioelement"*.

[43] C. C. Alvarez, M. E. Bravo Gómez, and A. Hernández Zavala. (2021). "*Hexavalent chromium: Regulation and health effects*". Journal of Trace Elements in Medicine and Biology, vol. 65.

[44] A. O. Lukina, C. Boutin, O. Rowland, and D. J. Carpenter. (2016). "*Evaluating trivalent chromium toxicity on wild terrestrial and wetland plants*". Chemosphere, vol. 162, pp. 355–364.

[45] A. M. Zayed and N. Terry. (2003). *"Chromium in the environment: factors affecting biological remediation*".

[46] D. Kimbrough, Y. Cohen, A. Winer, L. Creelman, and C. Mabuni. (1999). *"A critical assessment of chromium in the environment".* Critical reviews in environmental science and technology, vol 29, pp. 1-46.

[47] A. M. Jabonero and R. Gil Serra. (2021). "*Deposition of Thick Nanostructured Cr-based Coatings by HiPIMS*".

[48] T. L. Chou, S. Y. Yang, and K. N. Chiang. (2011). *"Overview and applicability of residual stress estimation of film-substrate structure"*. Thin Solid Films, vol. 519, no. 22, pp. 7883–7894.